Development of a Semi – Empirical Reaction Kinetic Model for PEM Fuel Cells

Dissertation

Submitted in partial completion of the degree MSc(Eng)Chem

Prepared by:

Adrian C. Fortuin

Prepared for:

Dr. Olaf Conrad

Dr. Pieter B.J. Levecque

Department of Chemical Engineering
National Hydrogen Catalysis Competence Centre

March 2013

PLAGIARISM DECLARATION

I certify that this submission is my own, unaided work, except for information obtained from literature sources. All sources of information have been adequately acknowledged and referenced. I have not received assistance from any other source in completing this submission.

Signed by candidate

Date: 27.05.2013

Adrian Fortuin

Dedicated to Kevin Simon Japp

May you forever rest in peace.

ACKNOWLEDGEMENTS

While I have been looking forward to writing this, perhaps I should keep this short and sweet. I did have fantasies of writing a long, elaborate short story to all those that I wish to extend my eternal gratitude to.

These last two years have been an interesting time for personal growth, maturity and of course doing research. The journey of self-growth is still on-going; however this work has seen its course. Hopefully someone else will find some inspiration in this particular topic and grow it to a mighty oak with me and all the other researchers studying the ever challenging oxygen reduction reaction. A mysterious mistress that may consume my academic life till I breathe my last breath.

Before I extend my gratitude to all those wonderful and important people, I think it would be proper to first thank those who have supported this work financially.

The financial assistance of the National Research Foundation (NRF) and further financial support from the Department of Science and Technology in the form of HySA/Catalysis Centre of Competence top-up bursary towards this research is gratefully acknowledged. Opinions expressed and conclusions arrived at, are those of the author and are not necessarily to be attributed to the NRF.

Now with the formalities aside, I wish to thank the special people in my own special way. To avoid any issue of who is more important than the other, I will thank people in groups and in alphabetical order. I'm trying to be a bit PC about it.

Colleagues

To the administrative staff (Debbie, Eloise and Lee-Anne), thank you for all your help when I needed to purchase chemicals or purchase something that was not necessarily research orientated. Thanks for the assistance when I needed to organise a social event or needed some clarification with regards to bureaucratic matters.

I would like to thank Prof. Hubert Gasteiger, Prof. Günther Scherer and Prof. Eric van Steen for the discussions around my work. Those discussions have assisted me in unlocking some of the mysteries of this research and without them this work would not have been possible.

To Jack, you still owe me an overseas academic trip, but thank you for seeing my potential and pulling me into such an awesome field. It was fantastic to have your support and keen interest in my academic future, thank you.

I would like to extend a special thank you to my supervisors: Olaf and Pieter. Olaf, your love for this work is truly contagious and I love your enthusiasm and excitement for the work that we are all doing. I really appreciate the caring and understanding that you have shown me, particularly when I was going through a rough patch. Your encouragement and absolute knowledge of fuel cells has inspired me to produce a piece of work that is of a high standard. I thank you for your open-door approach, your willingness to spoil us students and grow quality researchers. Thank you for putting us on the map and treating us to quality academics in the form of Prof. Hubert Gasteiger, Prof. Günther Scherer and Prof. Thomas Schmidt. You have provided us with all the tools necessary to blossom into great researchers. I look forward to our future discussions.

Pieter, you leave me speechless. Even though I infuriate you at times (we'll blame it on my youth), the discussions have been awesome. I have been extremely fortunate to learn

from such an incredible and insightful mind. Here's to the continued OCD nature of electrochemistry and electrocatalyst synthesis.

Family

To my mom, whom I affectionately call Mother, thank you for all your support and providing me with the fantastic opportunities to grow into such a know it all. Thank you for allowing me to explore my curiosities; whether it resulted in me sticking things in wall sockets, or making 'potions' with all your fancy cosmetics, or playing with that chemistry set you bought me. I will admit that I did get up to a lot of mischief, and it is surprising that I still have all my limbs and senses. You instilled a logical sensibility into me that resulted in me first investigating the possible implications before setting off some sort of 'explosion'. Thank you for allowing me to drift into the right direction, and instilling a good morals and beliefs.

To Carlos, Granny and Grandpa, and the Hunt family thanks for being there for Mother in her times of need. Indirectly you were there for me in my times of need. Although this is a short thank you, the more elaborate version will present itself at the conclusion of my PhD.

Friends and so forth

A short thank you to these very special people, you have all played a role in writing this thesis. All of you have been there to support me through this work, some of you have assisted with my personal growth, some of you have been there to listen to my rants about the thing that is annoying me on a particular day, some of you have put up with weirdness and some of you have just been there to add a little extra joy in my life. So: Bridgette, Candice, Cobus, Graham, Karthik, Lucinda, Nabeel, Ros and Sasha; dankie baie for all the great times and memories. Now for the PhD…, I'm going to need the continued support of you guys for that challenge.

THANK YOU MARC!

SYNOPSIS

In the drive to more sustainable energy production, polymer electrolyte fuel cells (PEFC) have been at the pinnacle of global research. One of the major drawbacks of PEFCs is the requirement for expensive noble metal catalysts (platinum and ruthenium). Furthermore 75% of the overpotential losses at the cathode are due to the activation of the oxygen reduction reaction (ORR).

To reduce the platinum content requirements and understand the cause of the large overpotential of the ORR, a fundamental understanding of the reaction mechanism and the manner in which it proceeds under different operating conditions is required.

Presently, there still remains a large debate in literature around the mechanism followed by the ORR.

This study developed a kinetic model from conventional kinetic isotherms and it is proposed that an associative adsorption mechanism occurs at a low overpotential resulting in the dissociation of the hydroperoxyl species determining the rate of the ORR at the cathode of the PEFC.

In order to explain the above phenomena a kinetic model was developed, based on the Eley-Rideal mechanism. Furthermore, experiments were conducted at different oxygen partial pressures and low potentials whereby the associative mechanism is believed to dominate. Under these conditions linear sweep voltammograms were recorded. Regression of the derived kinetic model, by using the values for oxygen partial pressure, applied overpotential and kinetic current allowed for the determination of the kinetic constant of a polycrystalline platinum catalyst for ORR.

The kinetic model described allows for a better understanding of the ORR for a specific range of oxygen partial pressures and overpotential regimes. It has proved the notion that oxygen adsorption is potential independent and that evaluating the kinetics under constant overpotential and constant absolute potentials results in a decoupling of the observed reactions. The constant ovepotential plots allow insight into the reaction proceeding, whilst the constant absolute potential allows insight into the activation of the reaction.

It has been recommended that spectator ion effects should be investigated and eliminated and the analysis should be conducted via in-situ testing. This will result in obtaining a more intimate understanding of the effect of the ORR on an operating PEFC.

It has further been recommended that the interaction of the oxygen orbitals on the platinum orbitals be investigated and understood through a more rigorous model to promote an indication of the large overpotential losses. With this in mind, catalyst can be developed to target and minimise the large overpotential losses.

TABLE OF CONTENTS

LIST OF FIGURES

LIST OF TABLES

NOMENCLATURE

Roman Symbol	**Unit**	**Description**
A	[cm^2]	geometric area
D	[cm^2/s]	diffusivity
H	[J/mol]	enthalpy, specific
I	[mol/L]	ionic strength
K	[-]	equilibrium constant
R	[Ω]	resistance
S	[mol/L]	solubility
S_{tot}	[mol/cm^2]	mole active sites per surface area
T	[K]	temperature
U	[V]	potential
a	[-]	species activity
c	[mol/L]	concentration
f	[1/V]	F/RT
i	[A]	current
$i_{0,s}$	[A/cm^2_{ECSA}]	specific activity
j	[A/cm^2]	current density
k	[1/s]	rate constant
k_s	[-]	salting coefficient
k’	[L.bar/mol]	Henry’s coefficient
n	[-]	number of electrons
p	[bar]	pressure, partial
r	[$mol/cm^2.s$]	rate of reaction
x	[-]	mole fraction

Greek Symbols	**Unit**	**Description**
α	[-]	transfer coefficient
γ	[-]	reaction order
δ	[cm]	diffusion layer thickness
η	[V]	potential, over
θ	[-]	oxygen coverage
	[-]	reaction site
ν	[cm^2/s]	kinematic viscosity
	[-]	stoichiometric coefficient
ω	[J] [rpm]	energy of adsorption rotation rate

Subscript index	**Description**
0	exchange current (density)
	reference state
ads	adsorbed species
c	cathode
e	electrolyte
K	kinetic
l	limiting

O	oxygen
	species O in $O + ne^- \rightleftharpoons R$
rds	rate determining step
Ω	ohmic

Superscript index	**Description**
0	reference state
*	reaction site

Constant	**Value**	**Unit**	**Description**
F	96,485	[C/mol]	Faraday's Constat
R	8.314	[J/mol.K]	Universal Gas Constant

Abbreviation	**Description**
CL	catalyst layer
CPET	combined proton and electron transfer
CV	cyclic voltammogram
ECSA	electrochemical surface area
GDL	gas diffusion layer
HOR	hydrogen oxidation reaction
HySA/Catalysis	Hydrogen Catalysis Competency Centre
LSV	linear sweep voltammetry

MEA	membrane electrode assembly
OCV	open circuit voltage
ORR	oxygen reduction reaction
PEFC	polymer electrolyte fuel cell
PGM	platinum group metals
RDE	rotating disk electrode
RF	roughness factor

CHAPTER 1

INTRODUCTION

Due to increased energy demands per capita, the need for sustainable and clean energy sources has become a pressing matter as fossil fuel reserves begin to dwindle. Furthermore, it can be inferred that more efficient power generators would be critical in curving tomorrow's technology to produce less environmentally harmful wastes and aid in addressing the larger energy demands.

Polymer electrolyte fuel cells (PEFC) show great promise as future energy conversion devices as they are not limited by Carnot efficiencies. Although the hydrogen fuel is still obtained via fossil fuels, PEFCs show higher efficiencies than internal combustion engines. Another alternative is batteries, however the recharge times and range are limiting factors.

It is firmly believed that hydrogen is the fuel of the future superseding fossil fuels (Barbir, 2005). The drive towards hydrogen fuels is the mere portability of the energy converter system, i.e. the fuel cell, which is of utmost importance for vehicular systems, telecommunications, computers, and many more; as well as the dramatic increase in the global oil price.

A key component of PEFCs is the platinum based catalyst. South Africa possesses ca. 95% of the world's Platinum Group Metal (PGM) reserves and mined ca. 75% of the world's platinum in 2010 (Loferski, 2011).

As a result of the drive towards a hydrogen economy and South Africa's abundant PGM reserves, the South African Department

of Science and Technology (DST) have initiated Hydrogen South Africa (HySA), a flagship R&D project. Within HySA, three different Competence centres (HySA/Catalysis, HySA/Infrastructure and HySA/Systems) have been set up to reach the aims of the project. Mintek and the Department of Chemical Engineering of UCT jointly host HySA/Catalysis (Hydrogen Catalysis Competency Centre). The Competence Centre in Catalysis has been tasked to address the commercialisation of low temperature PEFC system for (trans-)portable power in South Africa.

In order to reach the 2022 target of a portable power prototype, South Africa is required to build up its knowledge base in PEFCs. This project aims to gain a fundamental understanding of the oxygen reduction reaction (ORR) occurring at the catalyst surface of the fuel cell cathode. It is thus hypothesised that the OOH_{ads} species formation plays a role in the rate determining step of the ORR at low current. This study focuses on the surface reactions occurring on the platinum surfaces, excluding more complex dynamics provided by the catalysis layer. Understanding the kinetics from a classical catalysis view should lead to the development of more efficient and economical PEFCs strengthening South Africa's position in the global market.

CHAPTER 2

LITERATURE REVIEW

2.1 Background

2.1.1 Importance of Fuel Cells

The first question to arise is why is there so much interest in fuel cells as a whole?

With the decline in fossil fuels reserves and the increased awareness of global climate change the technology that affects the global population the most are transportation and electricity needs.

From the perspective of a South African: electricity supply is one of the most concerning challenges. The unreliable service delivery of electricity to homes in South Africa has arisen from a large expanse of the population and industry. A large portion of the population reside in rural areas where the electricity grid is inaccessible due to cable theft and vandalism, further hampering the development of those areas and the provision of essential services (viz. clinics and schools).

Due to the sparse population density, telecommunication backup power for cellular phone towers is required in remote locations so as to ensure a nationwide service. Such systems cannot rely on the electricity grid as telecommunication services are required in emergencies, therefore (trans)portable power is required to maintain this service.

Where the standard technology is diesel generators, these generators are susceptible to fuel theft and vandalism.

A means to address this scenario is to use fuel cell technology to provide power to basic services (vaccine refrigerators, power for schools, etc.)

HySA aims to address a global demand towards cleaner transportation and power needs, which is essential for economic growth of South Africa, as well as to address the challenges faced by the more remote locations within South Africa.

2.1.2 Basic Elements and Working of Fuel Cells

2.1.2.1 Elements

The essential components of a PEFC are illustrated in Fig. 2.1 below.

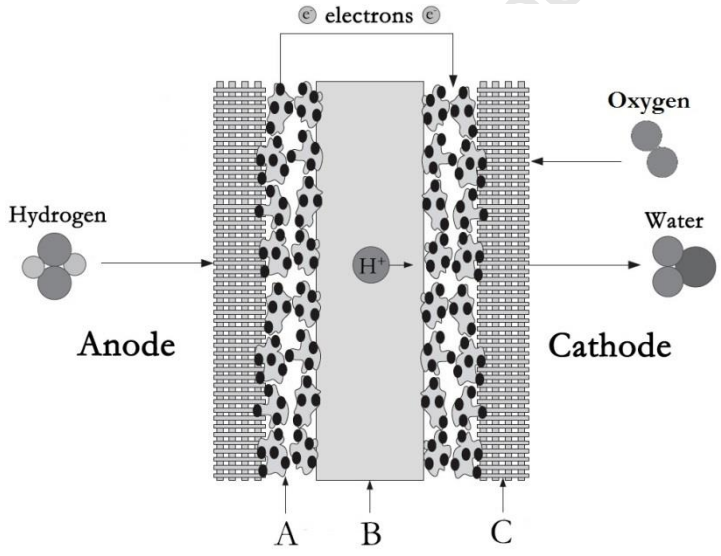

Figure 2.1: Illustration of a PEFC depicting the three key layers of the Fuel Cell and the reaction pathway. A: Catalyst Layer; B: Membrane; C: Gas Diffusion Layer (GDL)
Reproduced from Spiegel (2008)

The central component of a fuel cell is the membrane electrode assembly (MEA), which composes of a polymer electrolyte membrane to conduct protons from anode to cathode. On each side of the membrane is a supported platinum catalyst and a highly porous, electron conducting gas

diffusion layer (GDL) to distribute the reacting gases. The MEA is then sandwiched between bipolar plates, which act as a means to collect current and means for the gases to enter the fuel cell.

Fig. 2.1 depicts the operation of a PEFC. Humidified hydrogen is fed to the anode whereby it diffuses through the GDL and adsorbs onto the catalyst layer. The hydrogen oxidation reaction (HOR) occurs at the three-phase boundary, i.e. the point where the catalyst is in contact with both the membrane and the carbon electrode (eqn 2.1) and is wetted by water.

Anode: $$H_2 \xrightarrow{Pt/C} 2H^+ + 2e^- \qquad U^0 = 0.00\ V \quad (2.1)$$

The adsorbed hydrogen dissociates into protons and electrons, the protons are transported through the membrane (electrolyte) whilst the electrons travel via an external circuit. The protons and electrons recombine with oxygen (as air) at the cathode whereby the ORR occurs to form water (eqn 2.2).

Cathode: $$^1/_2 O_2 + 2H^+ + 2e^- \xrightarrow{Pt/C} H_2O \qquad U^0 = 1.23\ V \quad (2.2)$$

Combining the anode and cathode half reactions, the overall electrochemical process is as in eqn 2.3 below,

Overall: $$H_2 + {}^1/_2 O_2 \xrightarrow{Pt/C} H_2O + \text{heat} + \text{power} \qquad U^0 = 1.23\ V \quad (2.3)$$

2.1.2.2 Working Principle

The reactions are not as simple as depicted in the previous section. The anodic reaction is six to eight orders of magnitude faster than the cathodic reaction.

Furthermore, if one were to observe the open circuit voltage (OCV – defined as the measured potential with no load) of a PEFC in operation, the OCV would register at around 900 mV. This is far below that predicted by eqn 2.2. Anderson (2012) discusses that although many believe the reduced potential is due to the poisoning of the catalyst surface by OH_{ads}, it appears as if the actual reason is a thermodynamic limit imposed by a step in eqn 2.2 that does not involve a transferred electron.

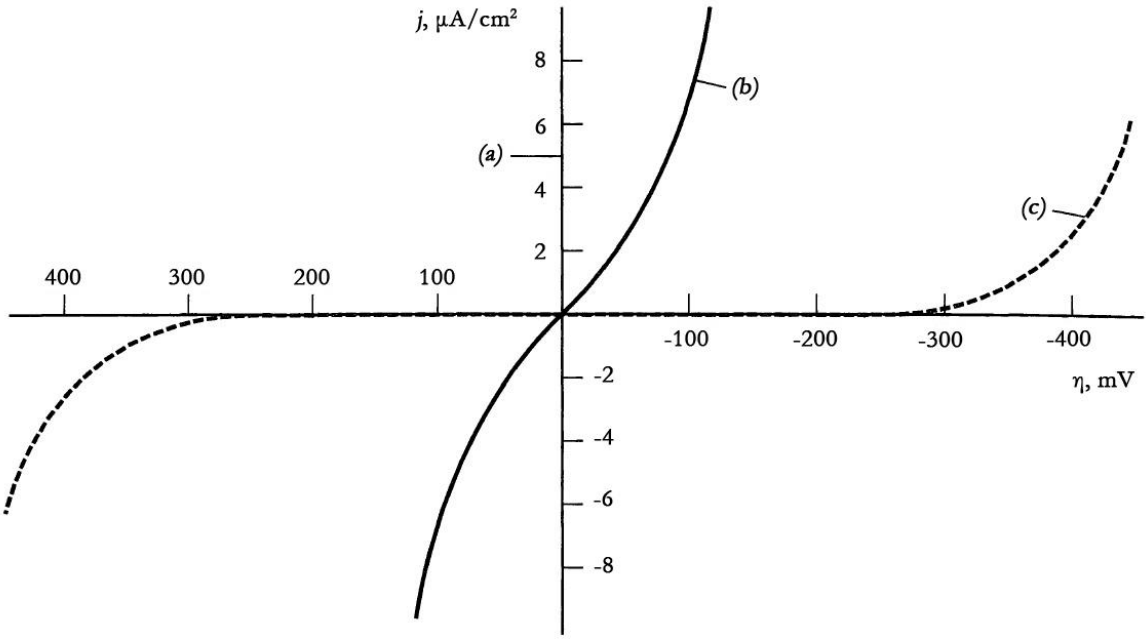

Figure 2.2: Exchange current density effect on the activation overpotential where (a) $j_0 = 10^{-3}$ A/cm^2 (b) $j_0 = 10^{-6}$ A/cm^2 (c) $j_0 = 10^{-9}$ A/cm^2. Each curve represents $O + e^- \rightleftharpoons R$, $\alpha = 0.5$ and $T = 298$ K
Reproduced from Bard and Faulkner (2001)

Fig 2.2 illustrates the large activation potential associated with the ORR (curve (c) is analogous to the ORR) which is typically thought to be approximately 400 mV (Neyerlin et al., 2007) from the theoretical potential of 1.23. The HOR,

however, has an activation overpotential of less than 5 mV (curve (a) is analogous to the HOR).

With all the associated losses, the typical operating range of a PEFC is 600 mV, which is approximately half the theoretical operating voltage. Thus, if the ORR activation potential can be reduced to 100 mV, so much more potential is available for electrical work. Therefore, the ORR remains the biggest challenge associated with PEFC, with large activation losses due to sluggish kinetics.

2.2 Catalyst Layer

2.2.1 Elements and Three Phase Boundary

The catalyst layers (CL) are the crux of the fuel cell's electrochemical reactions. In order for the CLs to effectively catalyse reactions, the CLs need to fulfil the following functions (Spiegel, 2008; Kucernak, 2011):

- Catalyst particles are to be connected with both the protonic conductor (membrane) and the electron conductor (GDL).
- The catalyst layer has to be porous to allow reactants and products to reach and leave the active catalyst sites respectively.
- The effective area of the catalyst layers needs to be much greater than the geometric area of the electrodes (i.e. Debe (2011) indicates that a surface enhancement factor of 47 – 145 cm^2_{Pt}/cm^2_{planar} is required depending on the catalyst loading), to ensure acceptable reaction rates and activity.
- The catalyst needs to show resistance to poisoning, in particular PEFC's running on reformate gas, are prone to CO poisoning.

- The catalyst needs to show good mechanical and chemical stability, i.e. needs to show minimal deactivation over time, needs to be corrosion resistant and sintering is to be avoided.

The catalyst typically comprises of platinum supported on carbon powders viz. Vulcan XC72R (Cabot), Black Pearls BP 2000, Ketjen Black Intl. or Chevron Shawinigan (Barbir, 2005). The catalyst layer needs to be prepared such that a three-phase boundary is developed; whereby the carbon support acts as the electron conductor, the ionomer/electrolyte acts as the proton conductor and the platinum particles acts as the catalyst (Fig 2.3), while void space needs to be present for transport of gases (reactants).

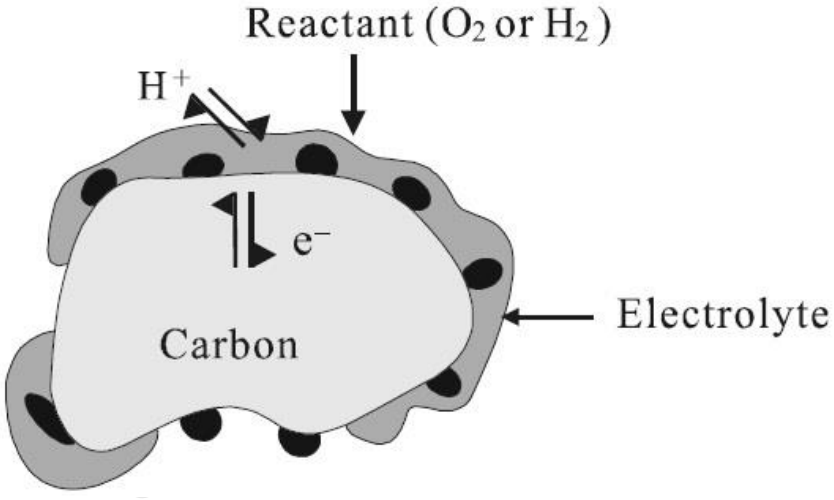

Figure 2.3: Three-phase boundary in the catalyst layer
Reproduced from Shen (2008)

The catalyst layer is sandwiched between the membrane and GDL, allowing for both protonic and electronic conduction. The carbon support acts as the electron conductor to the GDL and the hydrophilic areas (infused with Nafion® ionomer) of the catalyst layer act has the proton conductor to the membrane.

According to Kucernak (2011), the catalyst layer requires good water handling properties to aid proton conduction through the catalyst layer to and from the membrane. However, large quantities of water could lead to flooding, creating severe mass transport limitations. Therefore, it is important to have areas of hydrophobicity in the catalyst layer (as in the membrane) to transport water out and minimise the degree of flooding at high current densities.

2.2.2 Catalyst for ORR

Barbir (2005) has indicated that a platinum crystallite size of 4 nm or less ensures a large active surface area, provided it is finely dispersed on the support material. Furthermore, a 10 – 40 wt% ratio of platinum to carbon loaded to 0.4 mg/cm^2 MEA shows negligible change in published literature in the performance of a PEFC (Barbir, 2005), this is attributed to the active surface area of the catalyst remaining fairly unchanged. Table 2.1 indicates the loss of active area with increasing platinum to carbon ratios, which is attributed to increasing platinum crystallite size due to decreased dispersion. However, the above needs to be approached with caution as the work by Sheng *et al.* (2012) has shown that Pt/C crystallites tend to reach an optimum particle size of 5 nm because the kinetic rate of Ostwald ripening effects slows down, only then do the crystallites become stable.

Table 2.1: Platinum Active Area achieved using Pt supported on Ketjen Carbon Black

Reproduced from Barbir (2005)

wt.% Pt/C	Pt Crystallite Size [nm]	Active Area [m^2/g Pt]
40	2.2	120
50	2.5	105
60	3.2	88
70	4.5	62
Unsupported Pt black	5.5 – 6.0	20 - 25

Although, Pt/C is the most popular catalyst as indicated by Barbir (2005), recent developments have shown that platinum bimetallic electrocatalysts show more promise, particularly for the ORR (Watanabe *et al.*, 2012) because of the interactions of the transition metal with platinum in the ORR.

In a workshop presentation by Prof. Thomas Schmidt (2012) hosted by HySA/Catalysis five key points were highlighted in order to improve on the electrocatalyst activity of the ORR:

i. "Increase Pt loading.
ii. Increase Pt surface area.
iii. Increase $i_{0,s}$, e.g. increase temperature.
iv. Decrease surface coverage of spectator species.
v. Increase O_2 pressure."

Increasing Pt loading (i) is not a feasible option as there is a drive towards reducing the loading due to the cost of platinum. However, there still exists the possibility of new non-noble materials arising, which could show similar activity to platinum and thereby an increased loading may not be a problem. Caution would have to be exercised though, so as to ensure that the electrode is not too thick and thereby avoiding the creation of increased diffusion challenges.

Increasing the O_2 pressure (v) is not feasible either. There already exist challenges in storing hydrogen for transport services and the refuelling of hydrogen cylinders for remote fuel cell usage. The appeal of the PEFC is the fact that it uses atmospheric air, requiring one less complication in the commercialisation of the technology.

With points (i) and (v) being nullified, the only other options for increasing catalyst activity are points (ii), (iii) and (iv) of which all three usually need to be optimised simultaneously.

A lot of work has been conducted by studying the Pt(111) single crystal face, however, single crystal faces cannot be applied at a practical level due to changes that occur to the platinum crystallites in operation of a PEFC. Polycrystalline platinum (Pt_{poly}) gives one a better fundamental insight into the function of a continuous monolayer of Pt (as would be seen in an operating fuel cell) on its activity to reduce oxygen and is regarded as a benchmark to compare Pt catalysts to.

As mentioned above, one of the ways to increase Pt surface area is to alloy Pt with cheaper transition metals. Work by Stamenkovic *et al.* (2007) provides a good summation of work done on bimetallics with particular emphasis on the degree of d-band shifting influenced by the addition of a row IV transition elements.

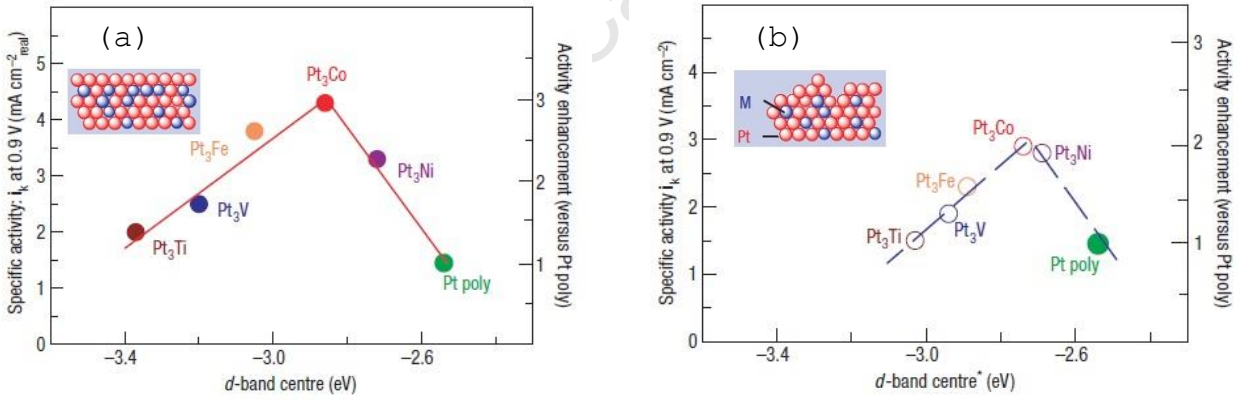

Figure 2.4: Experimentally Measured Specific Activities of the ORR on Bimetallic Platinum Surfaces in 0.1 M $HClO_4$ at 60 °C against the d-band centre for (a) Pt-skin and (b) Pt-skeleton
Reproduced from Stamenkovic *et al.* (2007)

The principle behind the above study is to reduce the amount of platinum used by coating a cheap and abundant metal. The surface area of platinum is increased, but the d-band centre is shifted favourably in order to alter the $4d_{3/2}$ and $4d_{5/2}$ orbitals of platinum (Watanabe *et al.*, 2012) to interact better with oxygen's 2p orbitals (Stamenkovic *et al.*, 2006).

The effect of the transition metals has varying effects on the ORR activity. For example, the metal alloys on the left of the volcano peak adsorb oxygen too strongly, whilst those on the right adsorb too weakly. It is worth noting that as one moves from left to right, the electronegativity of each transition element increases and this may be the key to predicting suitable alternative catalysts.

An interesting point of Fig 2.4 is the effect that the differences between a platinum-skeleton and platinum-skin has on the activity. The alloy arrangement obviously creates a difference in the electronic interaction between the two metals.

2.3 Catalyst Challenges

2.3.1 Durability and Contamination

Of the many challenges that face PEFCs: the presence of contaminanents, activity losses due to the ORR and start-stop/load cycling are considered the most troublesome.

Main contaminanets enter fuel cell via fuel. The most dominant contaminent is CO, as H_2 comes from reformate. CO is a huge concern for the anode as CO preferencially adsorbs on the catalyst surface over hydrogen, reducing the number of active sites available for reaction. On the other hand, chlorine contaminants may enter the cathode via the air stream (e.g. voltalie organic compounds or coastal air). Under electrochemical conditions, the presence of chlorine ions encourage an increase in Ostwald ripening and platinum dissolution thereby reducing the number of active sites (Pitois *et al.*, 2010; Baschuk and Li, 2003; Manasilp and Gulari, 2002; Li *et al.*, 2011; Baturina *et al.*, 2011; Zhang *et al.*, 2009).

Start-stop/load cycling creates a situation whereby Ostwald ripening prevails via platinum dissolution (Ferreira *et al.*, 2005). The mechanism of platinum dissolution is illustrated below.

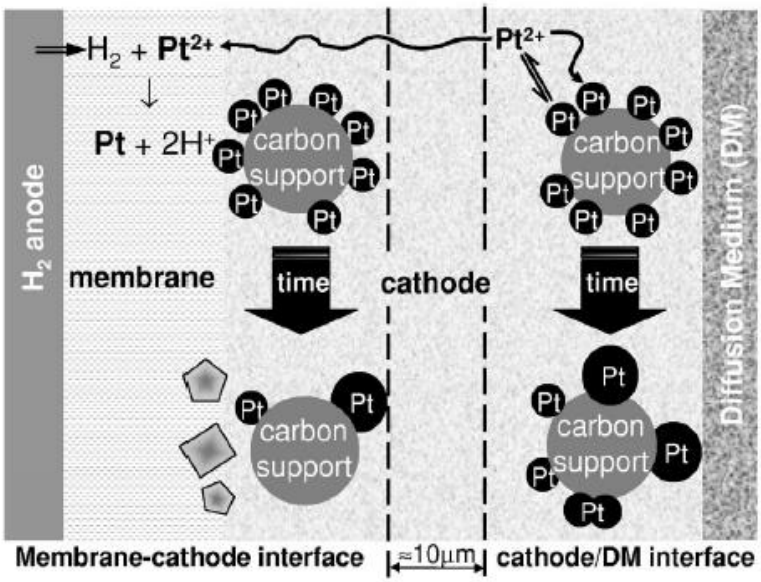

Figure 2.5: The mechanism by which platinum dissolution occurs leading to Ostwald ripening and the diffusion of platinum into the membrane and its subsequent reduction by H_2.
Reproduced from Ferreira *et al.* (2005)

Due to the presence of high voltages, the platinum Pourbaix diagram predicts the dissolution of platinum. The Pt^{2+} ions are mobile and capable of moving in the catalyst layer, even to the membrane via the ionomer present on the catalyst layer. By cycling the voltage between 600 – 1000 mV for 10,000 cycles, the degree of active platinum loss can be depicted by the loss in electrochemical surface area (ECSA), i.e. the area available for electrochemical reactions.

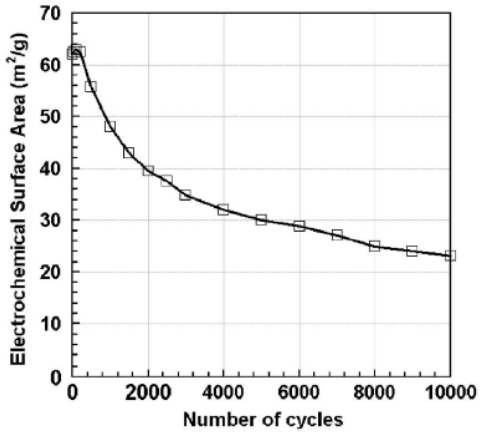

Figure 2.6: Cathodic platinum ECSA over 10,000 cycles between 600 – 1000 mV at 80 °C.
Reproduced from Ferreira *et al.* (2005)

2.3.2 Activity Losses

Currently, a major focus in PEFC research is on finding a suitable catalyst to reduce the activation losses associated with the ORR (Cui *et al.*, 2012; Adzic *et al.*, 2007; Zhou *et al.*, 2009; Lai *et al.*, 2010; Stolbov and Ortigoza, 2012; Ruvinskiy *et al.*, 2011; Greeley *et al.*, 2009; Zhang *et al.*, 2005).

State of the art PEFCs requires a platinum loading of ca. 0.4 mg_{Pt}/cm^2 at the cathode. This translates into ca. 0.5 g_{Pt}/kW, which is five times greater than that defined by the United States of America's DOE technical targets for 2015 (Gasteiger, 2012). With the above in mind, ORR catalyst activity has to show ten times greater improvement on the current technologies.

The system, does however, suffer from various losses. Hence the reversible cell potential (1.23 V) is not achieved. Fig. 2.7 below shows a fuel cell polarisation curve with the losses and the associated current density where they occur.

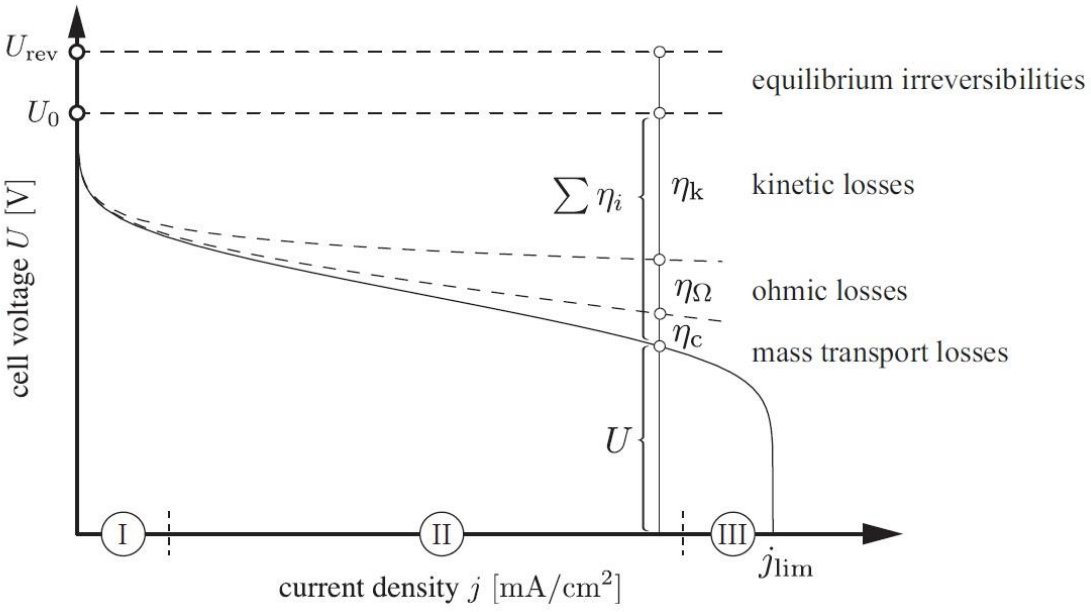

Figure 2.7: Polarisation Curve of a PEFC showing the three regions of electrical losses in an operating PEFC
Reproduced from Kramer (2007)

The various losses are attributed to the kinetic activation, ohmic losses and mass transport losses. Each loss has an associated overpotential which is the potential that deviates from the reversible potential. Eqn. 2.4 sums the associated cell potential with the various losses taken into consideration

$$U_{cell} = U_{rev} - iR_\Omega - \eta_{HOR} - |\eta_{ORR}| - iR_{H+} - \eta_{MT} \quad (2.4)$$

The kinetic losses to the system are due to overcoming the activation energy of the electrochemical reactions (η_{ORR} = 410 mV, η_{HOR} = <5 mV). The ohmic losses are due to ionic and electronic conductivity losses (η_Ω = 90 mV, η_{H+} = 18 mV), which are due to membrane resistance to proton flow and resistance of electron flow through the various conductors respectively. Finally, the mass transport losses are due to the use of air as a reactant and large amounts of water forming at the cathode, resulting in flooding (η_{MT} = 44 mV). Therefore, reactants have to diffuse through a second phase (namely water), which limits the rate considerably (Kucernak, 2011; Lamy, 2011; Baschuk and Li, 2000; Gasteiger, 2012).

As seen above, the ORR activation overpotential contributes to 75% of the total losses. In order to successfully develop a catalyst, the ORR needs to be understood at a fundamental level, i.e. how does the adsorbed O_2 molecule interact with the catalyst and react to form H_2O? From there an analysis can be conducted in order to design a more suitable catalyst with the increased activity required to meet the DOE targets. Modelling can assist in acquiring some of these insights.

2.4 Models for ORR

There remains much debate in literature as to the reaction pathway of the ORR at the atomic level (Keith and Jacob, 2010; Jacob, 2006). However, there appears to be a consensus that the Damjanovic mechanism (Fig. 2.8.) is followed and is in fact a very broad mechanism for the understanding of the ORR in acidic conditions over a large potential range (Vázquez-Huerta *et al.*, 2010; Antoine *et al.*, 2001; Sepa *et al.*, 1981; Damjanovic and Brusic, 1967).

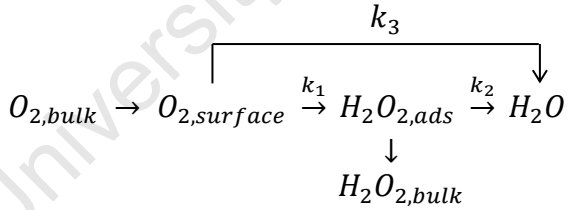

Figure 2.8: Damjanovic Mechanism for the Oxygen Reduction Reaction Reproduced from Vázquez-Huerta *et al.* (2010)

Furthermore, Jacob (2006) has strongly suggested that the ORR follows two main reaction pathways, namely the: (1) dissociative and (2) associative pathways. The dissociative mechanism (seen below as derived by Park *et al.* (1999)) involves the adsorption of molecular oxygen onto **two** vacant platinum sites followed by the dissociation of oxygen into two atomic oxygen species and further reaction to molecular water occurs.

Park *et al.* (1999) proposed the following dissociative mechanism for oxygen reduction by hydrogen to form water,

$$O_2 + 2* \rightleftharpoons 2O* \quad (2.5)$$

$$H + * \rightleftharpoons H* \quad (2.6)$$

$$H* + O* \rightleftharpoons OH* + * \quad (2.7)$$

$$H* + OH* \rightleftharpoons H_2O* + * \quad (2.8a)$$

$$2OH* \rightleftharpoons H_2O* + O* \quad (2.8b)$$

$$H_2O* \rightleftharpoons H_2O + * \quad (2.9)$$

On the other hand, the associative pathway (seen below as derived by Nørskov *et al.* (2004) involves the adsorption of molecular oxygen onto **one** vacant platinum site and reacts with a coupled proton and electron transfer (CPET) to form an adsorbed OOH_{ads} species and eventually molecular water (Jacob, 2006; Nørskov *et al.*, 2004).

The Keith and Jacob (2010) and Nørskov *et al.* (2004) proposed mechanism is shown below,

$$O_2 + * \rightleftharpoons O_2* \quad (2.10)$$

$$\mathbf{O_2* + (H^+ + e^-) \rightleftharpoons HO_2*} \quad \mathbf{(2.11)}$$

$$HO_2* + (H^+ + e^-) \rightleftharpoons H_2O + O* \quad (2.12)$$

$$O* + (H^+ + e^-) \rightleftharpoons HO* \quad (2.13)$$

$$HO* + (H^+ + e^-) \rightleftharpoons H_2O + * \quad (2.14)$$

$$H_2O* \rightleftharpoons H_2O + * \quad (2.15)$$

Both of the above pathways show similar energetics, however, the associative pathway shows the most favourable energetics (lower free energy) under gas phase reaction conditions as concluded by Jacob (2006) with Nørskov *et al.* (2004) concluding that both pathways can run in parallel, however the associative pathway dominates at potentials below 0.75 V (Ruvinskiy *et al.*, 2011). The energetics of the two pathways is depicted in Fig. 2.9. below:

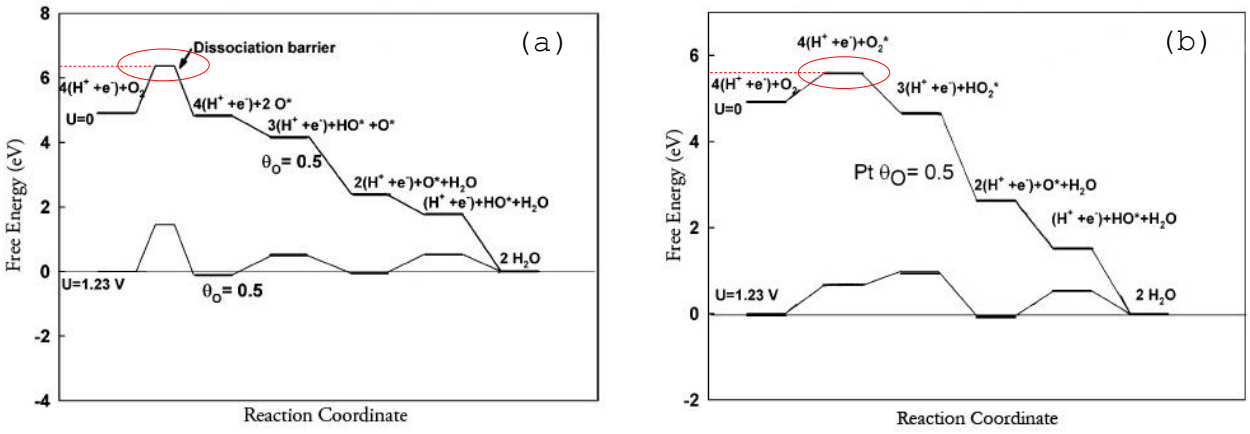

Figure 2.9: Free Energy Diagrams based on Density Functional Theory of the ORR for (a) the dissociative pathway and (b) the associative pathway with an oxygen coverage of 0.5

Reproduced from Nørskov *et al.* (2004)

In order to understand how the protons and molecular oxygen react, Keith and Jacob (2010) suggests that one of two possible mechanisms are possible, namely: (1) an Eley-Rideal mechanism or (2) a Langmuir-Hinshelwood mechanism. With the Langmuir-Hinshelwood mechanism both reactants adsorb onto the platinum surface and react, whereas the Eley-Rideal mechanism sees protons reacting from the electrolyte with adsorbed oxygen on platinum (see fig 2.10 for a visual explanation).

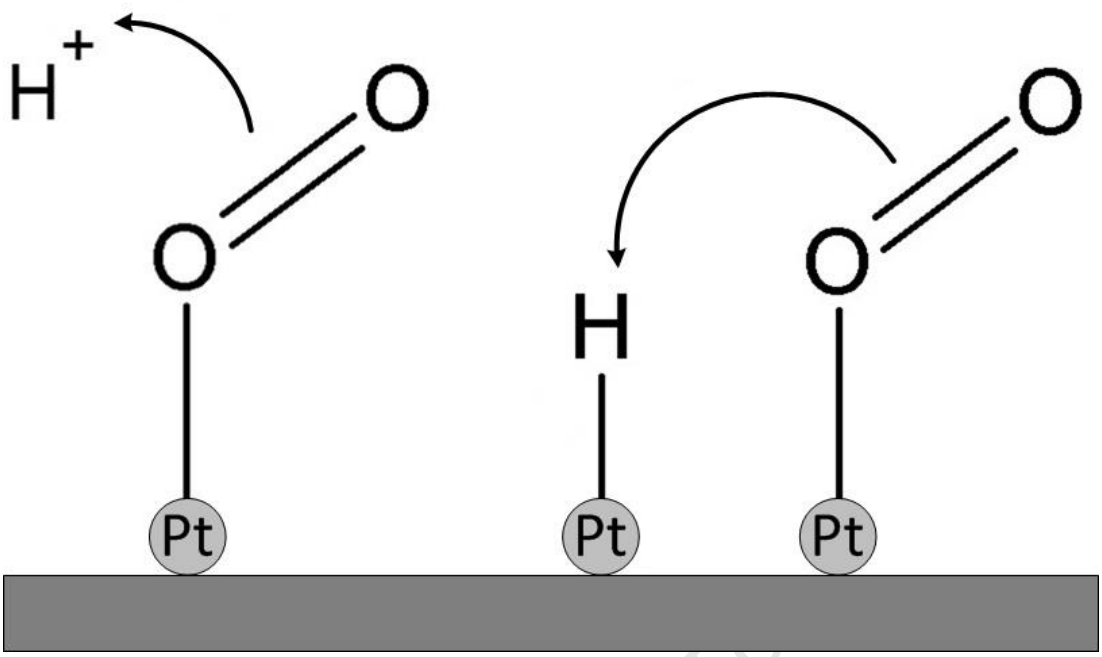

Figure 2.10: Visual representation of the Eley-Rideal mechanism (left) and the Langmuir-Hinshelwood mechanism (right)

Literature is divided on whether a Langmuir-Hinshelwood mechanism is followed or an Eley-Rideal; with Jacob (2006) and Park *et al.* (1999) leaning to a Langmuir-Hinshelwood mechanism and Nørskov *et al.* (2004), Antoine *et al.* (2001) and Anderson (2012) leaning to an Eley-Rideal mechanism.

Keith and Jacob (2010) show that at low electrode potentials Eley-Rideal mechanisms are more favourable over Langmuir-Hinshelwood mechanisms, however both mechanisms may run in parallel at high electrode potentials.

From the above, it appears as if both reaction pathways are applicable as well as both surface adsorption mechanisms. The key variable is the operating potential of the PEFC, thus the kinetics will differ at different conditions. This is supported by Song *et al.* (2007) who have stated that the rate determining step changes from the high potential range to the low potential range.

With regards to the rate determining step, it appears there is a unanimous agreement that the rate determining step of the ORR is the first "chemical" step regardless of the pathway, i.e., the first protonation of the adsorbed oxygen species (Keith and Jacob, 2010; Song *et al.*, 2007; Antoine *et al.*, 2001). However, Keith and Jacob (2010) indicate that there is disagreement over the proposed first "chemical" step. This fact is further strengthened by Song *et al.*'s (2007) findings that only at high electrode potentials the protonation of the adsorbed oxygen species is the rate determining step with the absence of a CPET. However, Song *et al.*'s (2007) conclusion would still hold for a CPET reaction as well.

This disagreement appears to be trivial, as most authors believe that the ORR follows a Damjanovic mechanism (associative mechanism), which intrinsically follows a CPET type of reaction. The fact is further supported by the contradiction of Keith and Jacob (2010) with the article published by Jacob (2006) earlier, who stated that the rate determining step for the associative pathway is the dissociation of the OOH_{ads} species into OH_{ads} and O_{ads} species. However, Jacob (2006) did conclude that the rate determining step for the dissociative pathway is the first CPET reaction as concluded by many other authors (Keith and Jacob, 2010; Song *et al.*, 2007; Antoine *et al.*, 2001).

Of the kinetic models developed, none really answer the pertinent question of which is the rate determining step (rds) of the ORR. There is still much focus to develop models based on conventional electrochemical derivations, viz. Tafel relationships and the derived Butler-Volmer equation.

Subramanian *et al.* (2012) has shown a modification of the Tafel kinetics equation and together with the inclusion of a Temkin isotherm approach, an oxygen coverage-dependent kinetic expression was developed.

$$i = i_0 \left(\frac{p_{O2}}{p_{O2,ref}} \right)^{\gamma} (1-\theta) \exp\left(\frac{-\alpha F \eta}{RT} \right) \exp\left(-\frac{\omega \theta}{RT} \right) \quad (2.16)$$

The above modification allows a little more insight into the ORR, but not from a mechanistic point of view. It rather gives an indication of the surface coverage of oxide species, which gives the point at which the reaction sees very low available sites for reaction.

The most comprehensive kinetic study was probably that presented by Ruvinskiy *et al.* (2011). The focus of the study was on the H_2O_2 pathway via the Yeager model, Damjanovic model and a simplified mathematical model.

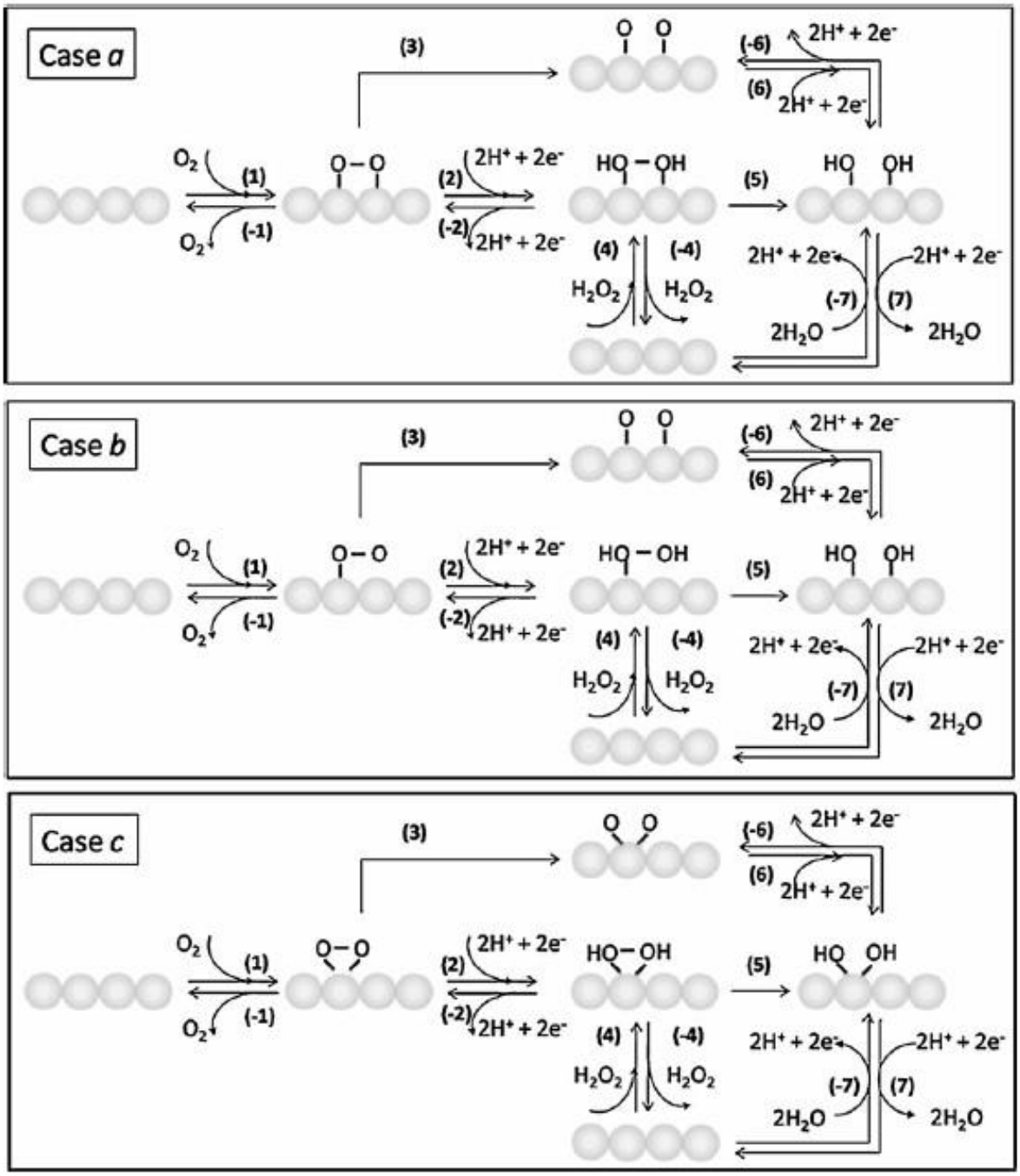

Figure 2.11: Schematic of the three ORR mechanisms studied by Ruvinskiy *et al.* (2011) where (a) Yeager Model, (b) Damjanovic Model, (c) Simplified Mathematical Model

Reproduced from Ruvinskiy *et al.* (2011)

$$\upsilon_{1a} = k_1[O_2](1 - 2\theta_{O2} - 2\theta_{H2O2} - \theta_O - \theta_{OH})^2 - k_{-1}\theta_{O2}$$

$$\upsilon_{1b,c} = k_1[O_2](1 - \theta_{O2} - \theta_{H2O2} - \theta_O - \theta_{OH}) - k_{-1}\theta_{O2}$$

$$\upsilon_2 = k_2\theta_{O2}\exp\left(\frac{-(1-\alpha)FE}{RT}\right) - k_{-2}\theta_{H2O2}\exp\left(\frac{\alpha FE}{RT}\right)$$

$$\upsilon_{3a,c} = k_3\theta_{O2}$$

$$\upsilon_{3b} = k_3\theta_{O2}(1 - \theta_{O2} - \theta_{H2O2} - \theta_O - \theta_{OH})$$

$$\upsilon_{4a} = k_4[H_2O_2](1 - 2\theta_{O2} - 2\theta_{H2O2} - \theta_O - \theta_{OH})^2 - k_{-4}\theta_{H2O2}$$

$$\upsilon_{4b,c} = k_4[H_2O_2](1 - \theta_{O2} - \theta_{H2O2} - \theta_O - \theta_{OH}) - k_{-4}\theta_{H2O2}$$

$$\upsilon_{5a,c} = k_5\theta_{H2O2}$$

$$\upsilon_{5b} = k_5\theta_{H2O2}(1 - \theta_{O2} - \theta_{H2O2} - \theta_O - \theta_{OH})$$

$$\upsilon_6 = k_6\theta_O\exp\left(\frac{-(1-\alpha)FE}{RT}\right) - k_{-6}\theta_{OH}\exp\left(\frac{\alpha FE}{RT}\right)$$

$$\upsilon_{7a} = k_7\theta_{OH}\exp\left(\frac{-(1-\alpha)FE}{RT}\right) - k_{-7}(1 - 2\theta_{O2} - 2\theta_{H2O2} - \theta_O - \theta_{OH}) \times \exp\left(\frac{\alpha FE}{RT}\right)$$

$$\upsilon_{7b,c} = k_7\theta_{OH}\exp\left(\frac{-(1-\alpha)FE}{RT}\right) - k_{-7}(1 - \theta_{O2} - \theta_{H2O2} - \theta_O - \theta_{OH}) \times \exp\left(\frac{\alpha FE}{RT}\right)$$

Figure 2.12: The elementary equations for the ORR mechanisms discussed by Ruvinskiy *et al.* (2011)

The derivation above is far more extensive than those previously mentioned. However, the derivation is a more elaborate version of the Butler-Volmer multi-electron transfer kinetic mechanism.

The issue of determining the intermediate species coverage is still not fully understood, but due to the elaborate system of equations, the intermediate species coverage can be calculated quite easily.

The rate equation for the ORR is reduced from those alongside and is represented below,

$$i_{ORR} = -FAS_{tot}(2\nu_2+\nu_6+\nu_7) \qquad (2.17)$$

Whilst all the above models are sound and convenient for extensive simulations of the PEFC operation, the above does not give adequate indication of the rds.

A proposed way forward, to which this work aims to contribute, is to use density functional theory (DFT) models as presented by Keith and Jacob (2010), as a starting point.

DFT can be used to derive a rate equation from conventional Langmuir isotherms and couple it with experimental data to find a suitable fit.

2.5 Measuring Kinetic Parameters

The developed rate equation, as described in chapter 4, has been derived as a function of oxygen partial pressure. Thus, with varying oxygen concentration the response current will be measured and analysed such that the exchange current i_0 can be regressed for.

Therefore one needs to have a basic understanding of oxygen from an experimental perspective as well as understand the physics behind the actual experimental methods.

2.5.1 The Complexities of Experimental Oxygen

Like any gaseous substance, oxygen is subject to various thermodynamic properties which hamper its solubility in a liquid medium. The three main variables which dictate oxygen solubility are: pressure, temperature and salt concentration. All discussions in this section is summarised from Hitcheman (1988).

2.5.1.1 Pressure Dependence

Because of the generally low solubility of oxygen in a solvent (typical mole fractions are on the ppm scale), Henry's law is an excellent approximation for oxygen solubility. The principle behind Henry's law shows, a linear relationship between the fugacity of the solute (oxygen) and the mole fraction of the solute.

$$p = k'c \tag{2.18}$$

At low pressures (i.e. absolute pressures in the vicinity of 1 atm) the fugacity and vapour pressure of the solute are equivalent. The generalised Henry's law eqn 2.18 relates oxygen concentration in solution to the partial pressure of oxygen above the solution, where *k'* is a system specific constant.

This allows for the ability to ascertain that the electrolyte is at the specified concentration related to the partial pressure.

2.5.1.2 Temperature Dependence

It is well known that as temperature increases, gas solubility decreases. As the temperature increases, both the solute and solvent become more excited and thus the solvent's ability to hold gases decreases considerably.

From a thermodynamic point of view the relationship can be described by the following equation,

$$\left(\frac{\partial \ln x_{O2}}{\partial T}\right)_{P,pO2} = \frac{\Delta H}{RT^2} \qquad (2.19)$$

However the above only holds for a relatively small temperature range between 0 °C and 50 °C.

The fact that temperature is raised to the second power (T^2) indicates the sensitivity of the oxygen saturation to temperature. Therefore accurate temperature control is required for reliable results.

2.5.1.3 Salt Concentration Dependence

Salt concentration dependency follows the same trend as that of temperature. As the electrolytic solution concentration increases, the solubility of oxygen decreases.

The relationship of solubility of oxygen in an electrolyte is as follows,

$$\ln\frac{S}{S_e} = k_s I \qquad (2.20)$$

where S and S_e are the solubilities of oxygen in water and the electrolyte respectively, k_s and I are the salting coefficient and ionic strength of the electrolyte under study. Thus the effect of oxygen solubility is dependent on the spectator ion in solution.

2.5.2 Theory of Rotating Disk Electrodes (RDE)

RDE employs a forced convection-hydrodynamic system to minimise mass transfer limitations, thereby giving us insight into the mechanisms of the reaction rate. The basic principle of the system is illustrated below:

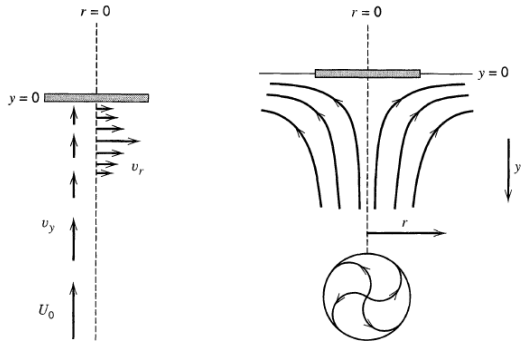

Figure 2.13: Graphical representation of the hydrodynamics of an RDE indicating the vectors and streamlines of a fluid.
Reproduced from Bard & Faulkner (2001)

Solving the convection-diffusion equations together with the velocity profile under steady-state conditions leads to the Levich equation,

$$i_{l,c}=0.62nFAD_O^{2/3}\omega^{1/2}\nu^{-1/6}c_o^* \quad (2.21)$$

where $i_{l,c}$ is the limiting cathode current, n is the number of electrons transferred, F is Faraday's constant, A is the geometric surface area of the electrode, D_O is the oxygen diffusivity in the electrolyte, ω is the rotation speed of the RDE, ν is the kinematic viscosity of the electrolyte and c_O is the concentration of dissolved oxygen in the electrolyte.

The diffusion layer thickness is evaluated as follows,

$$\delta_O=1.61D_O^{1/3}\omega^{-1/2}\nu^{1/6} \quad (2.22)$$

However, the Levich equation only applies to the fully mass transfer limited regime at the RDE.

It was noticed by experimental results that in some instances the Levich equation did not pass through the origin as predicted. This phenomena lead to the development of the Koutecky-Levich equation, which indicates mass transfer and kinetic resistances occurring in series,

$$\frac{1}{i}=\frac{1}{i_K}+\frac{1}{0.62nFAD_O^{2/3}\omega^{1/2}\nu^{-1/6}c_o^*} \quad (2.23)$$

where i_K represents the current under conditions of negligible mass transfer, i.e. the flow of current under kinetic limitations.

From the above theory and required parameters of the kinetic rate equations, a Koutecky-Levich plot is required to relate kinetic current (i_K) and oxygen concentration (c_{O2}).

Kocha & Takahashi (2010) showed that from linear sweep voltammetry (LSV) one can obtain the Koutecky-Levich plots from experimental data as illustrated below:

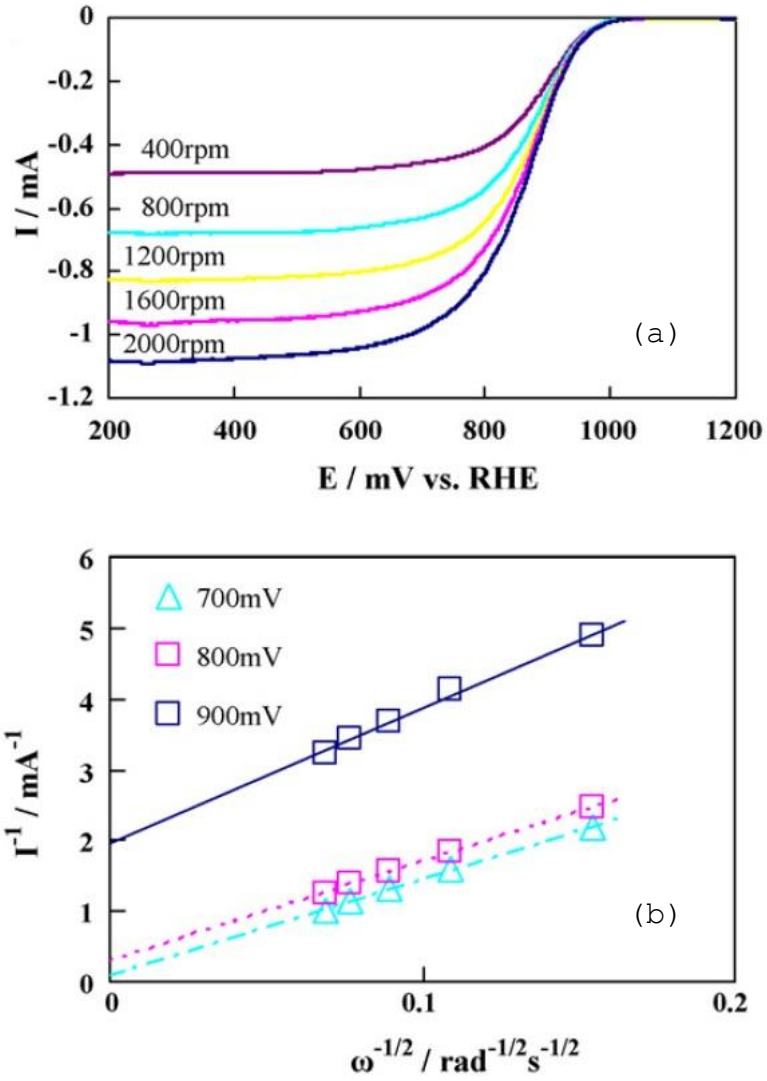

Figure 2.14: (a) Raw LSV data at various rotation rates under 100 % O_2 in 0.5 M H_2SO_4. (b) illustrates the consolidation of the LSV data into a Koutecky-Levich plot to study the kinetic current.
Reproduced from Kocha & Takahashi (2010)

At regions of high potential (low overpotential and low current density) kinetic limitations dominate, hence the determination of i_K at the y-intercept of the Koutecky-Levich plot (i.e. ω is ∞).

Therefore the experimental parameters are: U (applied potential), i (measured current), ω (set rotation speed of the RDE) and p_{O2} (set partial pressure of oxygen).

CHAPTER 3

EXPERIMENTAL

3.1 Electrochemical Measurements

All experiments were conducted in 0.5 M H_2SO_4 at 25 °C versus $Hg/HgSO_4$ reference electrode under saturated K_2SO_4. The temperature was controlled using a Lauda Alpha RA8 with a jacketed electrochemical cell. Accuracy of the circulating bath was verified by means of an analogue thermometer at random times during the experiments.

Before first use, all glassware was thoroughly cleaned by boiling in a 1:1 solution of H_2O_2:H_2SO_4 for 20 minutes and then soaking overnight. The boiled glassware was then rinsed 8 times in 18.2 MΩ.cm deionised water (nanopure). Thereafter, glassware was filled with 98 wt% H_2SO_4 (Kimix) overnight between runs and rinsed 8 times in nanopure water before experiments.

A fresh solution of 0.5 M H_2SO_4 was prepared for each set of experiments (1 set of experiments incl. CV, Background LSV and LSV for each oxygen partial pressure). 2.71 mL conc. H_2SO_4 (Kimix) was added to 25 mL of nanopure water and diluted to 100 mL in a volumetric flask. The solution was poured into a clean jacketed cell and deaerated with 99.999% Ar (Air Liquide) for a minimum of 30 minutes.

The Luggin capillary was filled with a solution of freshly prepared 0.5 M H_2SO_4 and the Hg/HgSO4 reference electrode was inserted. This was left to stand in the cell during dearation to ensure equilibrium between the cell electrolyte, the electrolyte in the Luggin capillary and the reference electrode.

A Pt mesh counter electrode was used. The counter electrode was flamed until glowing red to remove any contaminants. The mesh was then cooled under nanopure deionised water and submerged in the electrolyte.

Before each set of experiments a 3 mm polycrystalline Pt electrode (Metrohm) was first polished for 2 – 5 minutes in a figure 8 pattern using 6 µm diamond suspension (Buehler MetaDi® Supreme DF Diamond Suspension on VerduTex). The electrode was then rinsed with nanopure deionised water. The same process was repeated using alumina paste (Buehler MicroPolish) on Buehler MicroCloth, first polishing with the 1 µm, then 0.05 µm until bright platinum was observed.

The polished electrode was then submerged in nanopure deionised water and ultrasonicated for 30 min to remove any extra debris from the polishing process.

After rinsing with nanopure water, the electrode is then connected to an AutoLAB RDE (RDE-2) mechanism connected to an AutoLAB Potentiostat (PGSTAT302N). Data was collected using Nova 1.6 software.

All scans were conducted with continuous bubbling of the required gas. First a steady-state CV was recorded at 100 mV/s between 0.03 and 1.35 V vs. SHE and scanned for 30 cycles serving as an electrochemical cleaning step. This was then followed by 6 scans at 50 mV/s to determine the roughness factor (RF) of the polycrystalline electrode.

In order to correct for background current, an LSV was recorded between 0.15 and 1.20 V vs SHE at a sweep rate of 20 mV/s and rotations speeds of 400, 900, 1600, 2500 and 3600 rpm. Anodic scans were recorded for all rotation speeds except for 1600 rpm where cathodic and anodic scans were recorded.

The system was then purged with 99.998% O_2 (Afrox) for at least 30 minutes before recording ORR activity. Oxygen partial pressures (Ar was used to make up the differences) of 20%, 40%, 60%, 80% and 100% were selected using a mass flow controller system (Brooks) to obtain the kinetic current for model regression. The same scanning procedure as conducted for background current was used for ORR activity. The LSV recordings were all done in duplicate. An image of the experimental setup is depicted below in fig 3.1.

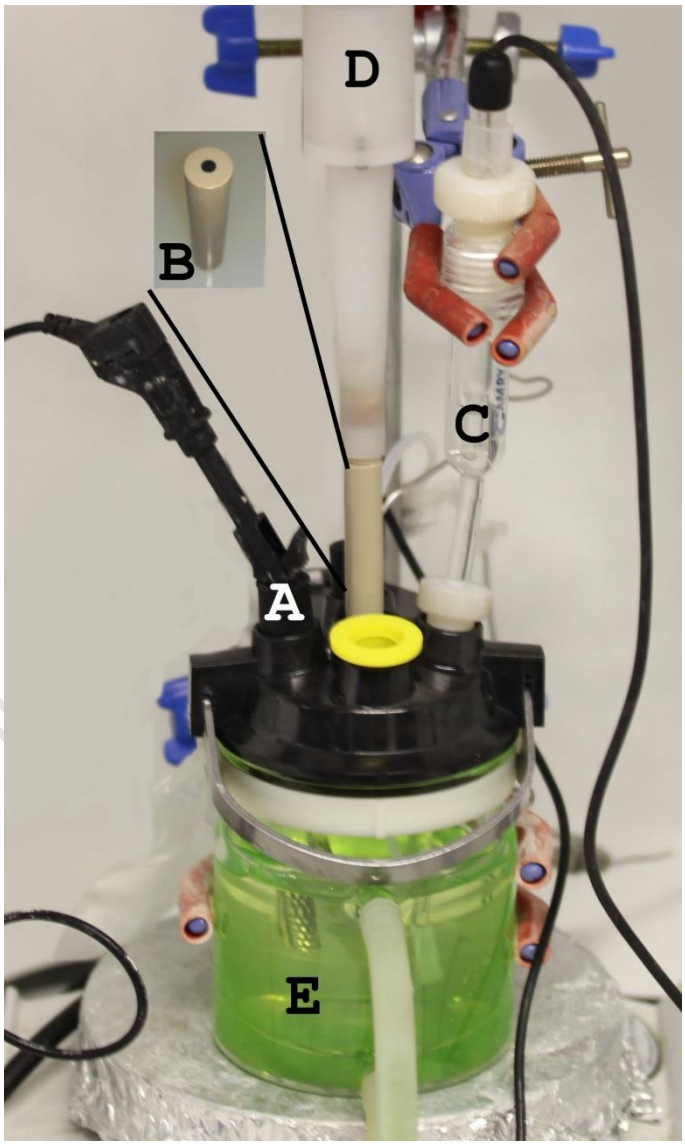

Figure 3.1: Experimental Setup where A: Pt mesh counter electrode, B: Polycrystalline Pt working electrode, C: $Hg/HgSO_4$ reference electrode, D: AutoLAB RDE and E: jacketed cell

3.2 Data Work-up and Model Regression

Koutecky-Levich plots were constructed from recorded data and the y-intercepts of the Koutecky-Levich plots were imported into MATLAB® at the various oxygen partial pressures. A least squares regression model was used with the built in "fminsearch" function.

"fminsearch" is based on the Nelder-Mead simplex method to minimise the error between the square of the experimental and model data.

CHAPTER 4

RESULTS AND DISCUSSION

4.1 Reproducibility of Results

In order to ensure good and reliable results, all experiments were conducted in five sets. Not only do the repeat experiments talk to reliability, but also to give proof that the trends observed are not outliers. Fig. 4.1 below illustrates the reproducibility of the CVs

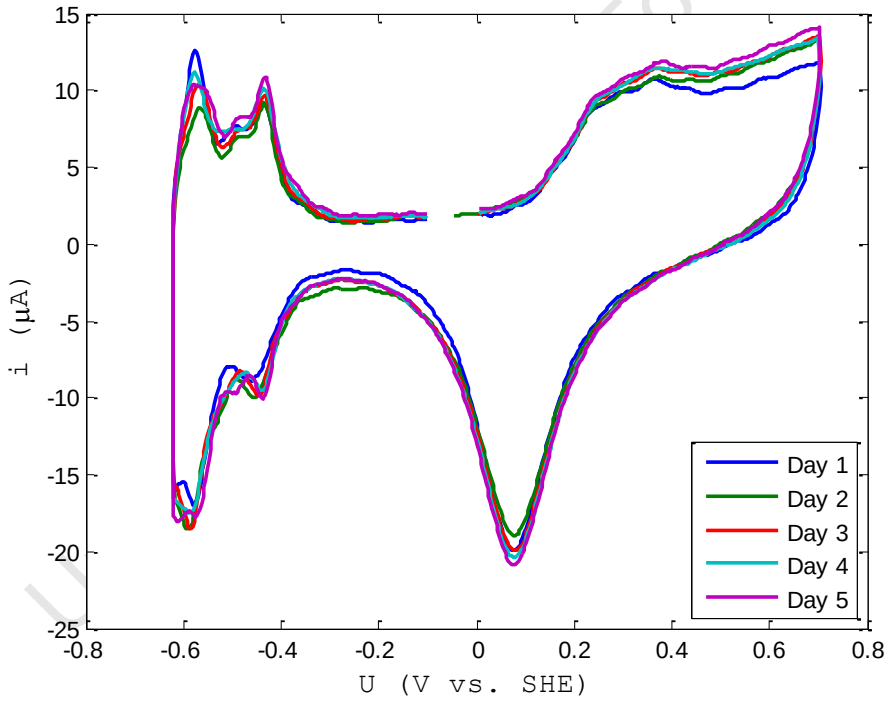

Figure 4.1: Individual CVs of polycrystalline Pt at a sweep rate of 50 mV/s at 25 °C in 0.5 M H_2SO_4 under Ar saturation depicting the reproducibility in the results.

All calculated data was derived from the curves in fig 4.1 above and fig 4.2 below. Looking at fig 4.1 the curves all fall on top of each other, with minor discrepancies. The roughness factors (RF) are all within experimental range of

each other, thus, the available surface area for reaction is fairly constant throughout the analysis.

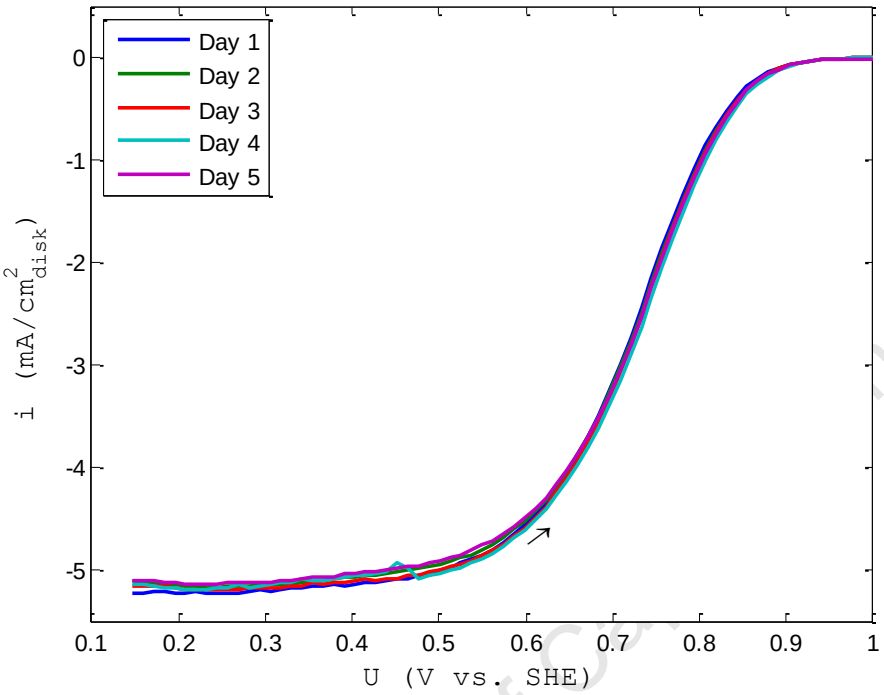

Figure 4.2: Individual background-corrected polarisation curves of ORR on polycrystalline Pt at a sweep rate of 20 mV/s and 1600 rpm at 25 °C in 0.5 M H_2SO_4 under 100% O_2-saturated depicting the reproducibility in the results.

This point is illustrated in fig 4.2 where all the LSVs fall on top of each other, with only minor deviations at low potential.

Applying the Levich equation, it is evident that full oxygen saturation was achieved, with limiting currents exceeding theoretical values as indicated in table 4.1 below.

Table 4.1: Theoretical versus experimental limiting currents (in A) of ORR in 0.5 M H_2SO_4 at 25 °C for 100 % oxygen partial pressure

	100%	
rpm	$I_{L,the}$	$I_{L,exp}$
3600	$4.52 \cdot 10^{-04}$	$5.33 \cdot 10^{-04}$
2500	$3.77 \cdot 10^{-04}$	$4.49 \cdot 10^{-04}$
1600	$3.01 \cdot 10^{-04}$	$3.63 \cdot 10^{-04}$
900	$2.26 \cdot 10^{-04}$	$2.76 \cdot 10^{-04}$
400	$1.51 \cdot 10^{-04}$	$1.88 \cdot 10^{-04}$

4.2 Experimental Results and Discussion: Observing the ORR

The CV in fig 4.3, an average of five separate sets, shows a clean and reproducible experimental environment. The reported RF of 2.24 is the range of that previously reported in literature for polycrystalline platinum (1.7 – 2.3).

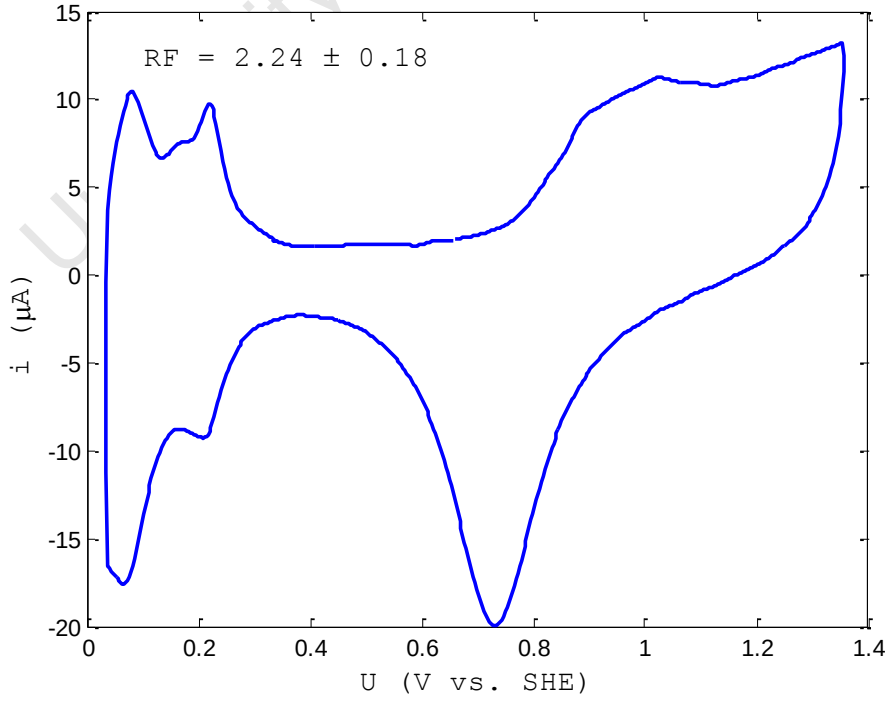

Figure 4.3: CV of polycrystalline Pt at a sweep rate of 50 mV/s at 25 °C in 0.5 M H_2SO_4 under Ar saturation

The above sees a clear onset of oxidation at 0.7 V in the positive sweep (forward sweep) with the formation of OH_{ads} species present. The large reduction peak between 0.5 – 0.9 V in the negative sweep (backward sweep) indicates a large available reduction current with a large surface available for ORR. This is indicated in fig 4.4 below.

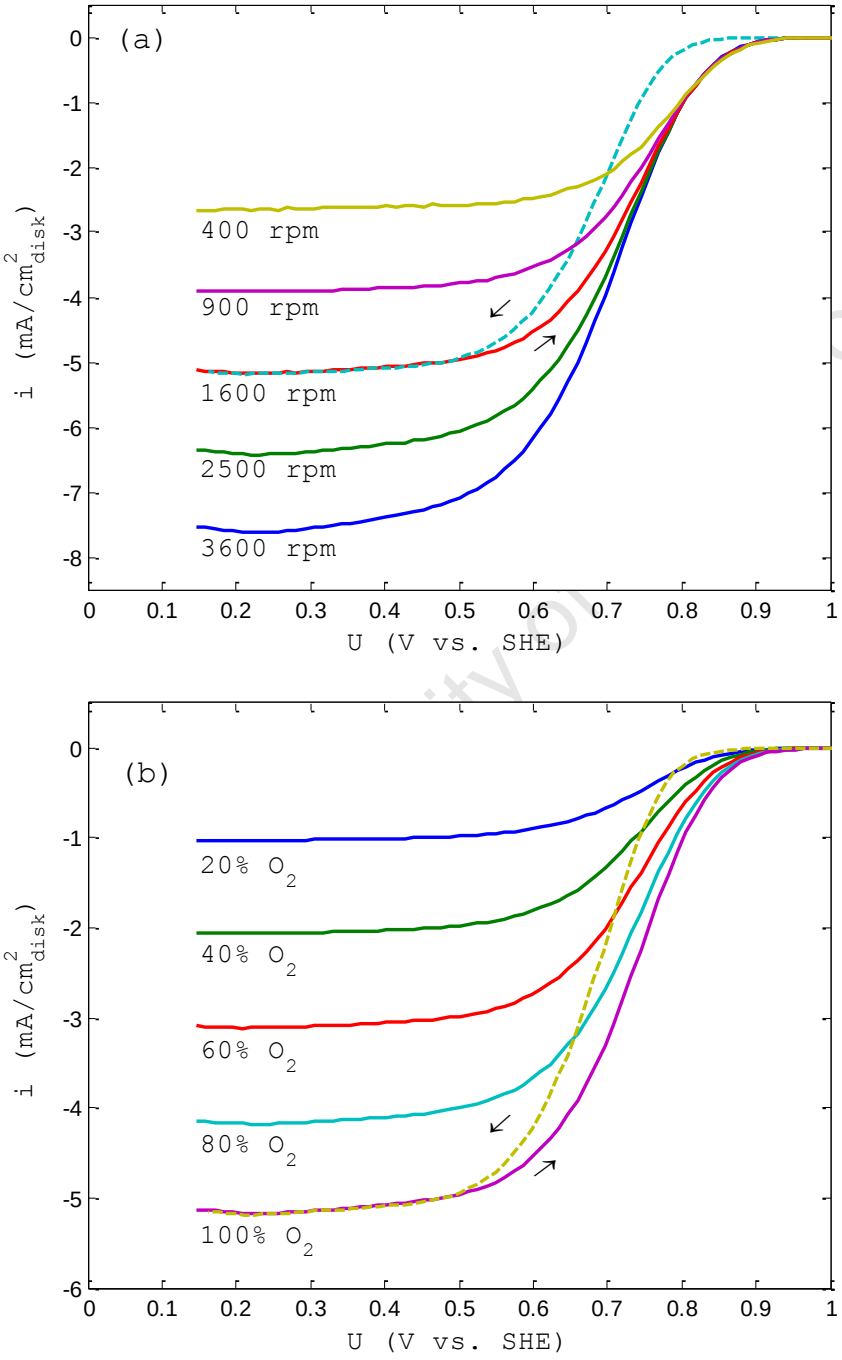

Figure 4.4: Background-corrected polarisation curves of ORR on polycrystalline Pt at a sweep rate of 20 mV/s at 25 °C in 0.5 M H_2SO_4 (a) under 100% O_2-saturated and (b) varied O_2 partial pressures at 1600 rpm. Solid lines represent upward going sweeps and only downward going sweeps at 1600 rpm are shown by the dotted line.

The curves in fig. 4.4 show the expected trends from a LSV scan (Sheng *et al.*, 2012; Paulus *et al.*, 2001). On closer inspection of the values presented in table 4.2 one will notice that the limiting currents are systematically slightly greater than that predicted by the Levich equation. However, the limiting currents are within accepted experimental variation for this type of experiments.

Table 4.2: Theoretical versus experimental limiting currents (in 10 x mA) of ORR in 0.5 M H_2SO_4 at 25 °C for varying oxygen partial pressures

	20%		40%		60%		80%		100%	
rpm	$I_{L,the}$	$I_{L,exp}$	$I_{L,the}$	$I_{L,exp}$	$I_{L,the}$	$I_{L,exp}$	$I_{L,the}$	$I_{L,exp}$	$I_{L,the}$	$I_{L,exp}$
3600	0.904	1.07	1.81	2.13	2.71	3.21	3.62	4.31	4.52	5.33
2500	0.753	0.906	1.51	1.80	2.26	2.71	3.01	3.63	3.77	4.49
1600	0.603	0.735	1.21	1.45	1.81	2.19	2.41	2.93	3.01	3.63
900	0.452	0.559	0.904	1.10	1.36	1.66	1.81	2.23	2.26	2.76
400	0.301	0.365	0.603	0.740	0.904	1.11	1.21	1.49	1.51	1.88

With the above data the Levich plot in fig. 4.5 indicates a good fit with the experimental limiting currents passing through the origin of the graph.

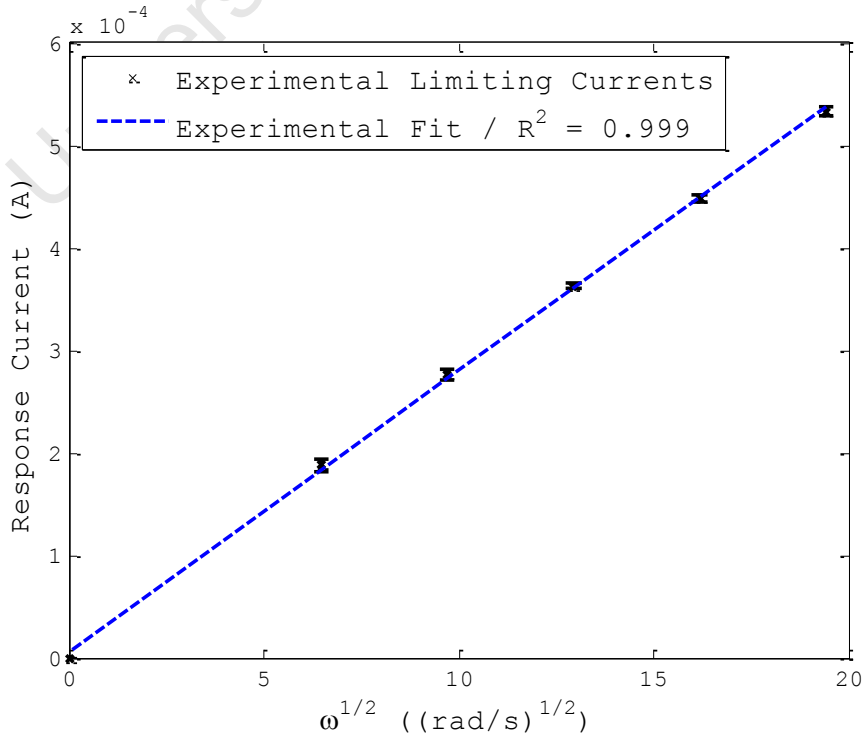

Figure 4.5: Levich plot for 100% O_2 saturation in 0.5 M H_2SO_4 and 25 °C

The above phenomenon is evident as a curve fitted through the limiting currents at the various rotation speeds results in 4.7 electrons transferred using the constants in table 4.2 below:

Table 4.3: Physical parameters for Levich plot
Reproduced from Song and Zhang (2008)

Electrolyte	**O_2 diffusion coefficient, cm^2/s**	**Electrolyte kinematic viscosity, cm^2/s**	**O_2 solubility, mol/cm^3**
0.5 M H_2SO_4, 25 °C and 1 bar O_2	$1.4 \cdot 10^{-05}$	0.010	$1.1 \cdot 10^{-06}$

The question now arises, why is it observed that 4.7 electrons are transferred? It was believed that perhaps, the solubility data of O_2 was recorded at a different altitudes or the temperature of the cell was not 25 °C as believed.

Experiments were conducted using a dissolved oxygen meter (Mettler Toledo O_2 Transmitter 4100) to test if the observed oxygen solubility is correct for the system under study. The results showed the same value as depicted in table 4.3.

Once the above was proven not be the source of the systematic error, the Levich equation (eqn 2.21) was reassessed to determine the possible source of error.

$$i_{l,c}=0.62nFAD_O^{2/3}\omega^{1/2}\nu^{-1/6}C_o^* \qquad (2.21)$$

Where all values are either constants or are set by the experimental equipment. The only terms which could be the

cause of the difference from 4.0 electrons measured are the diffusivity and kinematic viscosity terms.

Because of the difference, the number of electrons transferred was also verified using the Tafel equation below,

$$\log i = \log i_0 + \frac{\alpha n F}{2.3RT}\eta \qquad (4.1)$$

Applying eqn 4.1 to the recorded data of 100 % O_2 partial pressure at 1600 rpm, a Tafel slope of 72 mV/dec was found resulting in a value of 4.2 electrons transferred with a value of 1 for α. If one takes into account that no IR correction was done on the data the results from the Tafel slope clearly indicate that the reaction rates measured are for the full conversion to water.

Because there is only a discrepancy with the Levich equation, the source of the systematic error is most likely due to the value assigned to oxygen diffusivity or kinematic viscosity. However, the viscosity term is fairly constant due to the dilute nature of the acid and the constant temperature at which the cell is operating. It is assumed that electrolyte follows the properties of a Newtonian fluid, hence the effect of rotating the electrode in the electrolyte does not affect the viscosity.

The only remaining source of error is that associated with the diffusion coefficient. Because of the hydrodynamic behaviour of a RDE experimental setup, the convectional diffusion of oxygen could be drastically different from that quoted in literature. There are vastly different methods of measuring diffusivity and all seem to give a different result, although in an electrochemical environment the diffusivity can be calculated on the fact that 4 electrons are transferred for the ORR.

And indication of the variances in diffusion coefficients can be observed for the diffusion of oxygen in water as tabulated in table 4.4 from Kinoshita (1992).

Table 4.4: Diffusivity of Oxygen in Water at 25 °C and 1 atm
Reproduced from Kinoshita (1992)

Electrolyte	Temperature (°C)	O_2 Pressure (atm)	Diffusion Coefficient (cm^2/s)
H_2O (Pure)	25	1	$1.9 \cdot 10^{-05}$
H_2O (Pure)	25	1	$1.7 \cdot 10^{-05}$
H_2O (Pure)	25	1	$2.9 \cdot 10^{-05}$
H_2O (Pure)	25	1	$2.0 \cdot 10^{-05}$

As can be seen in table 4.3 there is a variance of as much as 41% between measured diffusivities of the oxygen in the same electrolyte under the same conditions.

Based on the discrepancies around the oxygen diffusivity and assuming that 4.0 electrons were transferred in fig 4.4, perhaps the oxygen diffusion coefficient should be updated to $1.8 \cdot 10^{-05}$ cm^2/s for future references.

4.3 Model Results and Discussion: A Proof of Damjanovic's Theory

4.3.1 Model Derivation

With the literature stated in chapter 2, it is evident that one needs an understanding of mechanistic nature of the ORR. In order to understand tunability of platinum, a study of the kinetic behaviour of the ORR on a polycrystalline surface is required. This study may give some insight into what aspects of the ORR mechanism require focus from the point of view of HySA/Catalysis' research interests.

The aim of this project is to take more unconventional approach to the answer the question by applying classical catalysis methods to derive a kinetic equation based on well-studied isotherms. The resultant is the derivation of an equation using the Langmuir isotherm and an Eley-Rideal approach on a continuous platinum surface.

The thought process and hypothesised rate equation is summarised below with a few alternative rate models available for comparison (however, the comparisons to these alternative models will not be discussed or analysed further).

The starting point is the Butler-Volmer equation. This equation has been derived for a general system regardless of the reactants or electrocatalyst used. The simplest Butler-Volmer multi-electron transfer mechanism is as follows (Bard and Faulkner, 2001),

$$i = nFAk^{0}_{rds}\ [C_{O2*}\exp(-\alpha f\eta)\ -\ C_{HO2*}\exp(\{1-\alpha\}f\eta] \qquad (4.2)$$

The problem with the above equation is the complication of measuring the exact coverage of the adsorbed oxygen and hydroperoxyl species. Thus, equation 4.2 is not a suitable approach to determining the rds.

A more conventional approach is to determine the exchange current density using Tafel kinetics. However, the equation does not give clear indication of the rds.

$$i = i_0\left(\frac{p_{O2}}{p_{O2,ref}}\right)^{\gamma}\exp\left(\frac{-\alpha F\eta}{RT}\right) \qquad (4.3)$$

The only real information of value is the determination of the reaction order, which could provide some minor insight into a potential mechanism.

In deriving the model for this work from classical catalysis methods, the first and most important assumption is the use of a Langmuir isotherm. It is well known that Langmuirian conditions are such that only a monolayer of adorbates forms, adsorption and desorption follow the same mechanism, the surfaces are energetically homogeneous and there are no interactions with neighbour adsorbates. The Langmuirian assumptions fit well with the associative mechanism and the assumption is supported by both Keith and Jacob (2010) and Anderson (2012).

Furthermore, by the fact of the Langmuir assumptions, the Eley-Rideal mechanism is the best approach. The fact that typical Pt/C is typically covered by ionomer and the ORR only takes place on water-wetted platinum sites, it is safe to assume that protons react with oxygen from the bulk and do not first adsorb onto platinum sites.

With the above two assumptions being stated, the kinetic equation has been derived using equations 2.10 – 2.14, where equation 2.11 is the rds. The exclusion of water desorption is negligible for the conditions of study (equation 2.15), i.e. U ≥ 0.8 V (this will be proven).

The hypothesised rate equation is derived below (see fold out, last page, for a summary of the symbols used below):

For eqn 2.11 being the rds, we have

$$-r_{2.11} = k_{2.11}\left(\theta_{OOH,ads} - \frac{\theta_{O2,ads} c_{H+}}{K_1}\right) \qquad (4.4)$$

∴ each of the steps (2.10, 2.12, 2.13 and 2.14) are in equilibrium with each other as their rates are considered to be much faster than in 2.11:

$$\theta_{O2,ads} = K_{2.10} p_{O2} \theta \quad (4.5)$$

$$c_{H2O} \theta_{O,ads} = K_{2.12} \theta_{OOH,ads} c_{H+} \quad (4.6)$$

$$\theta_{OH,ads} = K_{2.13} \theta_{O,ads} c_{H+} \quad (4.7)$$

$$c_{H2O} \theta = K_{2.14} \theta_{OH,ads} c_{H+} \quad (4.8)$$

Rearranging eqns 4.5 – 4.8 and solving for $\theta_{OOH,ads}$, we see that

$$\theta_{OOH,ads} = \frac{c_{H2O}^2 \theta}{K_{2.12} K_{2.13} K_{2.14} c_{H+}^3} \quad (4.9)$$

Preforming a site balance on all the available sites, viz. θ, $\theta_{OOH,ads}$ and $\theta_{O2,ads}$ and making θ the subject of the formula

$$\theta = \frac{1}{1 + K_{2.10} p_{O2} + c_{H2O}^2 / K' c_{H+}^3} \quad (4.10)$$

Substituting 4.10 into 4.9 and 4.5 and subsequently substituting into 4.4, we have

$$-r_{OOH} = \frac{k_{2.11}}{1 + K_{2.10} p_{O2} + c_{H2O}^2 / K' c_{H+}^3} \left(\frac{c_{H2O}^2}{K' c_{H+}^3} - \frac{K_{2.10} p_{O2} c_{H+}}{K_{2.11}} \right) \quad (4.11)$$

However, from the Nernst equation we see

$$\eta = \frac{1}{4f} \ln \frac{a_{O2} a_{H+}^4}{a_{H2O}^2} \quad (4.12)$$

assuming the activity of H_2O is unity, i.e. 1, the concentration of protons is made the subject of the formula

$$c_{H+} = \left(\frac{1}{p_{O2}} \exp(4f\eta) \right)^{1/4} = \beta \quad (4.13)$$

Substituting 4.13 into 4.11, assuming H_2O is unity based on the experimental setup, applying transition state theory and

relating rate to current we have the hypothesised rate equation below

$$i_{ORR} = \frac{4FAi_0 \exp\left(-\alpha \frac{\eta}{f}\right)}{1 + K_{2.10} p_{O2} + {}^{1}/_{K'\beta^3}} \left(\frac{1}{K'\beta^3} - K'' p_{O2} \beta\right) \qquad (4.14)$$

4.3.2 Model Regression

Although the above model is a simplified approach, it is rigorous enough to extract relevant kinetic data from experimental data.

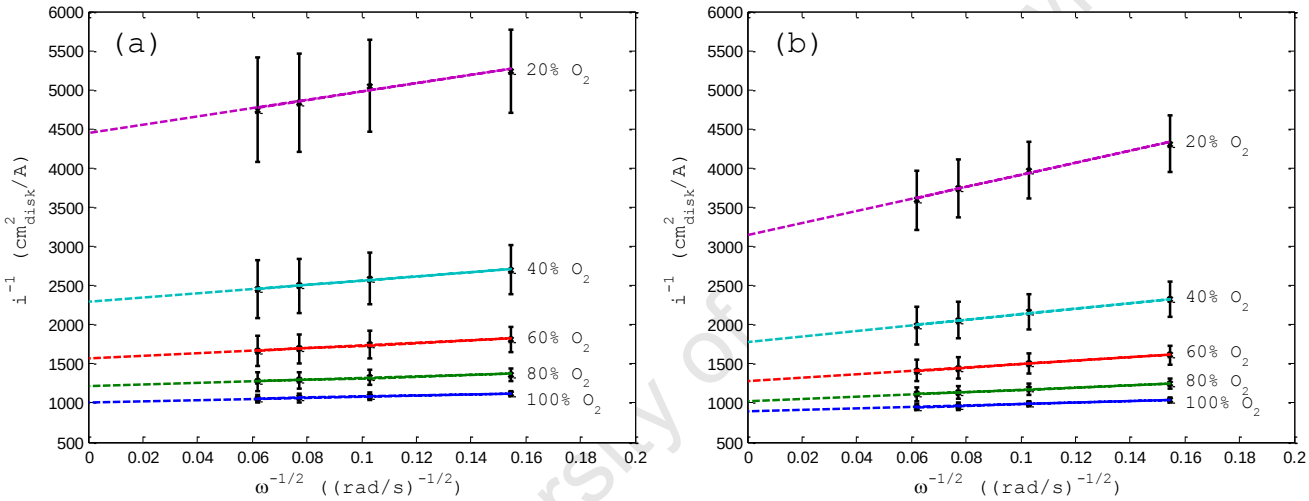

Figure 4.6: Koutecky-Levich plots at varying oxygen partial pressure at (a) 800 mV absolute potential and (b) 430 mV overpotential in 0.5 M H_2SO_4 and 25 °C.

Using the experimentally recorded LSVs, the Koutecky-Levich plots can be calculated as seen in fig. 4.6. However, two scenarios are observed: (a) Constant applied potential of 800 mV vs SHE (i.e. variable overpotential). As mentioned above, the equilibrium potential for the ORR is different at different oxygen partial pressures. This can be seen from the Nernst equation (eq 4.12). The consequence of a constant applied potential is therefore that the actual overpotential will be different at every partial pressure setting ($U-U_0$, with U constant and U_0 different for every overpotential). (b) Constant overpotential of 430 mV (i.e. variable applied potential). Since the equilibrium potential changes

at every oxygen partial pressure, obtaining a constant overpotential can only be done by varying the applied potential ($U-U_0$ needs to be constant, U_0 changes with changing overpotential, therefore U needs to change as well).

Although the trends in the Koutecky-Levich plot are as expected, there is a significant difference in the kinetic current between the constant absolute potential (4.6a) and constant overpotential (4.6b).

The constant overpotential curve sees a larger response current at each partial pressure, which is postulated to be due to more reaction steps being observed, i.e. more electron transfer steps. The constant absolute potential is not as informative, but does give valuable data as to the activation of the reaction and perhaps allows a little more insight into the first electron transfers. However, there is no real literature to support these claims; more research needs to be conducted to prove these hypotheses.

Using the kinetic currents, the exchange current density would be regressed using the derived models. The two most striking phenomena that can be observed from fig 4.7 is the curvature of the constant overpotential curves and the linearity of the oxygen adsorption step (see appendix A for the derived equation).

The curvature is a fairly easy phenomenon to explain, the constant absolute potential curves are linear because of the proportionality between the oxygen partial pressure and potential. The constant overpotential curves, however, show proportionality between the oxygen partial pressure and the Nernstian equation 4.12.

The more interesting phenomenon is the linearity of the oxygen adsorption curves. This linearity may be attributed to

the simple nature in which oxygen adsorbs onto the surface of the catalyst. Because the adsorption of oxygen is potential independent as discussed by Keith and Jacob (2010), there should be no curvature to the curve regardless of whether or not constant absolute potential or constant overpotential has been plotted. This is a sound proof of the potential independence of the oxygen adsorption mechanism.

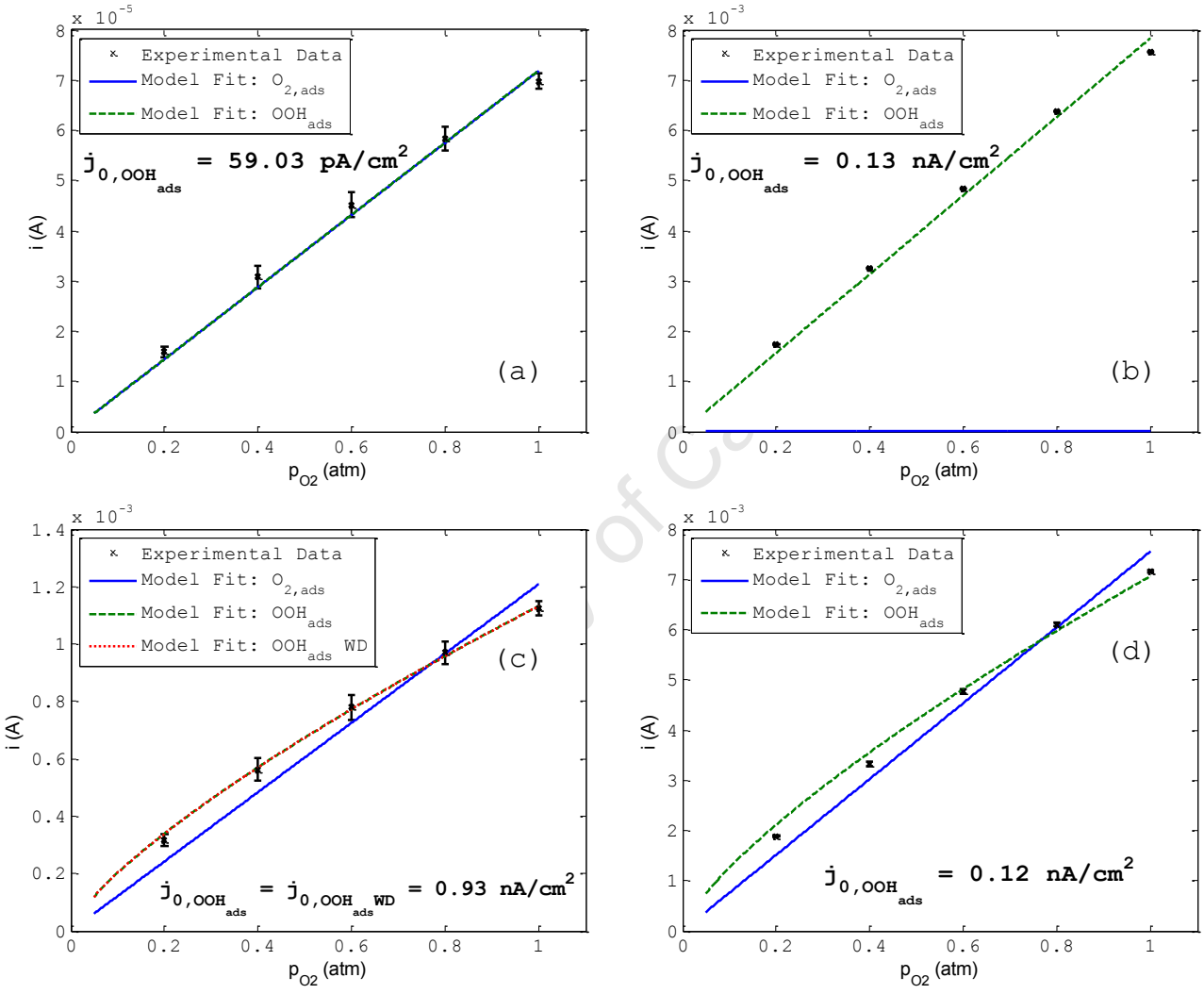

Figure 4.7: Regressed fit to derived rate equation for experimentally derived kinetic current for (a) constant absolute potential of 800 mV, (b) constant absolute potential of 700 mV, (c) constant overpotential of 430 mV and (d) constant overpotential of 530 mV in 0.5 M H_2SO_4 and 25 °C.

Keeping in mind the assumptions associated with the use of Langmuir isotherm, the desorption mechanism of water should follow the same principle of oxygen adsorption, i.e. it

should be potential independent. The phenomenon is once again observed (although not shown on all plots, it holds true for all) in fig 4.7c. The water desorption (WD) inclusion into the rate equation as postulate by Keith and Jacob (2010) has no effect on the regression and fit of the rate equation (equation 4.14). Both Nørskov *et al.* (2004) and Keith and Jacob's (2010) proposed mechanisms overlay.

Comparing fig 4.7a and fig 4.7b, the exchange current density for the rds appears to increase. As postulated above, this may be attributed to the fact that in fig 4.7a the reaction hasn't been activated, the presence of adsorbed oxygen is overwhelming, but the first combined proton and electron transfer (CPET) has not begun to dominate. At 700 mV the reaction appears to be proceeding at more rapid pace, with the effects of oxygen adsorption becoming negligible.

An interesting observation is the comparable exchange current density between fig 4.7b and 4.7d. Perhaps at 700 mV mass transfer limitations are becoming prominent or (and the more likely reason) the rds has shifted. This is in agreement with many authors who have observed a shift in the rds at varying potentials (Ruvinskiy *et al.*, 2011; Song *et al.*, 2007; Keith and Jacob, 2010).

However, fig 4.7c tells a different story. At constant overpotential of 430 mV (which is fig 4.7a's equivalent) the first CPET appears to be proceeding quite well, with an exchange current density close to that reported in literature of 1 nA/cm^2 (Kinoshita, 1992). The differences between 4.7a and 4.7c may be attributed to the fact that the first CPET actually occurs at a constant overpotential of 430 mV, but fig 4.7a illustrates the instant of activation and fig 4.7c indicates the reaction dominating. Thermodynamically, the few millivolts that separate the two scenarios could be indicative of different potitions on the energy potential diagram i.e. just before and just past the transition state.

Previous work conducted at HySA/Cataysis by Madala (2012) suggested that the maximum allowable surface coverage of intermediate species does not exceed 0.25 monolayers. For this work, this obviously raised the question of, what is the effect of surface coverage of OOH_{ads} formation based on the Langmuir isotherm? Table 4.5 indicates that in the instance of more OOH_{ads} being present on the surface of the catalyst site, the associated exchange current density increases.

Table 4.5: Exchange Current Density dependence on OOH_{ads}

OOH_{ads} Coverage	Exchange Current Density (nA/cm^2)
0.05	0.98
0.10	1.02
0.15	1.07
0.20	1.11
0.25	1.16

The above gives one an indication that if more OOH_{ads} could be formed on the Pt surface, there would be more available for further reaction. However, due to the slow nature of OOH_{ads} formation, a small fraction of the species is only ever present, being rapidly consumed in the next intermediate step.

The data in table 4.5 seems to suggest that OOH_{ads} formation could possibly be the rds.

4.3.3 Concluding Remarks

As discussed above, the application of a classical catalyst model can be derived and applied to an electrochemical environment.

From the plots in fig 4.7 there is clear evidence of the potential independence of the adsorption of oxygen on the

platinum surface, however, a more interesting conclusion is the decoupling nature of using constant absolute potential versus constant overpotential indicating of the decoupling between the activation of the reaction and the reaction proceeding.

CHAPTER 5

CONCLUSIONS AND RECOMMENDATIONS

From the data presented in Chapter 4, there is clear evidence that a conventional kinetic isotherm can be applied to an electrochemical environment.

There is further proof that oxygen adsorption is potential independent as discussed by Keith and Jacob (2010) with the hydroperoxyl species formation determining the rate of reaction.

A decoupling effect was observed by evaluating the rate equation under constant absolute potential and constant overpotential. Constant absolute potential gives an indication of the activation of the formation of hydroperoxyl species at 800 mV, whilst constant overpotential gives an indication of the reaction proceeding at 430 mV.

A clear observation is the shift in the rds at 700 mV absolute and 530 mV overpotentials as explained by their comparable exchange current densities. However, the hydroperoxyl formation still appears to be a factor in the rds, it appears as if there are multiple rds at those particular voltages.

Although this is not a rigorous model, it is a first step in understanding the ORR. The above results have been informative in terms of the nature of the ORR and has given new light on the inner workings, however further work needs to be conducted in order to eliminate the many assumptions. A more rigorous model would provide the necessary information to tackle the elusive nature of how the ORR actually proceeds.

Before delving into a more rigorous study of the ORR, further work first needs to be conducted in order to understand the influence of spectator ions on the results. An alternative is to conduct the experiments under in-situ conditions to fully understand the effects of the ORR on an operational PEFC.

Further a more fundamental study should be conducted on the interactions of the oxygen orbitals with platinum orbitals. Conducting such a study in combination with a general micro-kinetic model over the entire potential range would lead to a deeper understanding of the role of the catalyst in reducing molecular oxygen. Such work would lead to better engineering of catalysts for the ORR and how inclusion of transition metal alloys or doping agents to the support will affect the observed ORR rate.

The novelty of this approach to understanding electrocatalyst kinetics should lead to more fundamental advances in catalyst development for PEFCs, giving researchers another technique in order to meet the DOE targets.

REFERENCES

Adzic, R. R.; Zhang, J.; Sasaki, K.; Vukmirovic, M. B.; Shao, M.; Wang, J. X.; Nilekar, a. U.; Mavrikakis, M.; Valerio, J. a. & Uribe, F. (2007), "Platinum Monolayer Fuel Cell Electrocatalysts", Topics in Catalysis, 46, pp. 249-262.

Anderson, A. B. (2012), "Insights into Electrocatalysis", Physical Chemistry and Chemical Physics, 14, pp. 1330-1338.

Antoine, O.; Bultel, Y. & Durand, R. (2001), "Oxygen reduction reaction kinetics and mechanism on platinum nanoparticles inside Nafion®", Journal of Electroanalytical Chemistry, 499, pp. 85-94.

Barbir, F. (2005), "PEM Fuel Cells: Theory and Practice", Elsevier Academic Press.

Bard, A. J. & Faulkner, L. R. (2001), "Electrochemical Methods: Fundamentals and Applications", 2nd ed. Massachusett, John Wiley & Sons, Inc.

Baschuk, J. J. & Li, X. (2000), "Modelling of polymer electrolyte membrane fuel cells with variable degrees of water flooding", Journal of Power Sources, 86, pp. 181-196.

Baschuk, J. J. & Li, X. (2003), "Modelling CO poisoning and O2 bleeding in a PEM fuel cell anode", International Journal of Energy Research, 27, pp. 1095-1116.

Baturina, O. a.; Epshteyn, A.; Northrup, P. a. & Swider-Lyons, K. E. (2011), "Insights into PEMFC Performance Degradation from HCl in Air", Journal of the Electrochemical Society, 158, pp. B1198-B1198.

Cui, C.; Gan, L.; Li, H.-H.; Yu, S.-H.; Heggen, M. & Strasser, P. (2012), "Octahedral PtNi Nanoparticle Catalysts: Exceptional Oxygen Reduction Activity by Tuning the Alloy Particle Surface Composition", Nano letters, 12, pp. 5885-5889.

Damjanovic, A. & Brusic, V. (1967), "Electrode kinetics of oxygen reduction on oxide-free platinum electrodes", Electrochimica Acta, 12, pp. 615-628.

Debe, M. K. (2011), "Effect of Electrode Surface Area Distribution on High Current Density Performance of PEM Fuel Cells", Journal of the Electrochemical Society, 159, pp. B53-B66.

Ferreira, P. J.; la O', G. J.; Shao-Horn, Y.; Morgan, D.; Makharia, R.; Kocha, S. & Gasteiger, H. a. (2005), "Instability of Pt/C Electrocatalysts in Proton Exchange Membrane Fuel Cells", Journal of the Electrochemical Society, 152, pp. A2256-A2256.

Gasteiger, H. A. 2012. *Electrocatalyst Challenges for Low-Temperature Fuel Cells*. CATSA 2012. Cape Town.

Greeley, J.; Stephens, I. E. L.; Bondarenko, A. S.; Johansson, T. P.; Hansen, H. A.; Jaramillo, T. F.; Rossmeisl, J.; Chorkendorff, I. & Nørskov, J. K. (2009), "Alloys of Platinum and Early Transition Metals as Oxygen Reduction Electrocatalysts", Nature Chemistry, 1, pp. 552-556.

Hitcheman, M. L. (1988), "Measurement of Dissolved Oxygen", Krieger Pub Co.

Jacob, T. (2006), "The Mechanism of Forming H2O from H2 and O2 over a Pt Catalyst via Direct Oxygen Reduction", Fuel Cells, 6, pp. 159-181.

Keith, J. A. & Jacob, T. (2010), "Theoretical Studies of Potential-Dependent and Competing Mechanisms of the Electrocatalytic Oxygen Reduction Reaction on Pt(111)", Angewandte Chemie International Edition, 49, pp. 9521-9525.

Kinoshita, K. (1992), "Electrochemical Oxygen Technology", New Jersey, John Wiley and Sons, Inc.

Kocha, S. S. & Takahashi, I. (2010), "Examination of the activity and durability of PEMFC catalysts in liquid electrolytes", Journal of Power Sources, 195, pp. 6312 - 6322.

Kramer, D. 2007. "Mass transport aspects of polymer electrolyte fuel cells under two-phase flow conditions". Dr. -Ing., Technischen Universität Bergakademie Freiberg.

Kucernak, A. 2011. *Diagnostic Methods in PEM Fuel Cells*. HySA Catalysis: PEM Fuel Cell Catalyst and MEA Preparation and Charaterisation. Cape Town. University of Cape Town: Department of Chemical Engineering.

Lai, F. J.; Chou, H. L.; Sarma, L. S.; Wang, D. Y.; Lin, Y. C.; Lee, J. F.; Hwang, B. J. & Chen, C. C. (2010), "Tunable properties of PtxFe1-x electrocatalysts and their catalytic activity towards the oxygen reduction reaction", Nanoscale, 2, pp. 573-581.

Lamy, C. 2011. *Introduction to Electrocatalysis in Low Temperature Fuel Cells*. HySA Catalysis: PEM Fuel Cell Catalyst and MEA Preparation and Charaterisation. Cape Town. University of Cape Town: Department of Chemical Engineering.

Li, H.; Wang, H.; Qian, W.; Zhang, S.; Wessel, S.; Cheng, T. T. H.; Shen, J. & Wu, S. (2011), "Chloride contamination effects on proton exchange membrane fuel cell performance and durability", Journal of Power Sources, 196, pp. 6249-6255.

Loferski, P. J.: U.S. Geological Survey. (2011). Platinum - Group Metals. [WWW]. Available from: http://minerals.usgs.gov/minerals/pubs/commodity/platinum/mcs-2011-plati.pdf [Accessed 10 March 2011].

Madala, T. 2012. "Prediciting Surface Coverage from DFT on Pt(111)". MSc(Eng), University of Cape Town.

Manasilp, A. & Gulari, E. (2002), "Selective CO oxidation over Pt/alumina catalysts for fuel cell applications", Applied Catalysis B: Environmental, 37, pp. 17-25.

Nørskov, J. K.; Rossmeisl, J.; Logadottir, A.; Lindqvist, L.; Kitchin, J. R.; Bligaard, T. & Jónsson, H. (2004), "Origin of the Overpotential for Oxygen Reduction at a Fuel-Cell Cathode", The Journal of Physical Chemistry B, 108, pp. 17886-17892.

Park, Y. K.; Aghalayam, P. & Vlachos, D. G. (1999), "A Generalized Approach for Predicting Coverage-Dependent Reaction Parameters of Complex Surface Reactions: Application to H2 Oxidation over Platinum", The Journal of Physical Chemistry A, 103, pp. 8101-8107.

Paulus, U. A.; Schmidt, T. J.; Gasteiger, H. A. & Behm, R. J. (2001), "Oxygen reduction on a high-surface area Pt/Vulcan carbon catalyst: a thin-film rotating ring-disk electrode study", Journal of Electroanalytical Chemistry, 495, pp. 134-145.

Pitois, A.; Pilenga, A. & Tsotridis, G. (2010), "CO desorption kinetics at concentrations and temperatures relevant to PEM fuel cells operating with reformate gas and PtRu/C anodes", Applied Catalysis A: General, 374, pp. 95-102.

Ruvinskiy, P. S.; Bonnefont, A. & Savinova, E. R. (2011), "Further Insight into the Oxygen Reduction Reaction on Pt Nanoparticles Supported on Spacially Structured Catalytic Layers", Electrocatalysis, 2, pp. 123-133.

Schmidt, T. J. 2012. *Electrocatalysis in Polymer Electrolyte Fuel Cells*. HySA/Catalysis Workshop. University of Cape Town.

Sepa, D. B.; Vojnovic, M. V. & Damjanovic, A. (1981), "Reaction intermediates as a controlling factor in the kinetics and mechanism of oxygen reduction at platinum electrodes", Electrochimica Acta, 26, pp. 781-793.

Shen, P. K. (2008), "PEM Fuel Cell Catalyst Layers and MEAs", *In:* Zhang, J. (ed.) *PEM Fuel Cell Electrocatalysts and Catalyst Layers: Fundamentals and Applications,* 2nd ed. London: Springer, pp.

Sheng, W.; Chen, S.; Vescovo, E. & Shao-Horn, Y. (2012), "Size Influence on the Oxygen Reduction Reaction Activity and Instability of Supported Pt Nanoparticles", Journal of the Electrochemical Society, 159, pp. B96-B96.

Song, C.; Tang, Y.; Zhang, J. L.; Zhang, J.; Wang, H.; Shen, J.; McDermid, S.; Li, J. & Kozak, P. (2007), "PEM fuel cell reaction kinetics in the temperature range of 23–120°C", Electrochimica Acta, 52, pp. 2552-2561.

Song, C. & Zhang, J. (2008), "Electrocatalytic Oxygen Reduction Reaction", *In:* Zhang, J. (ed.) *PEM Fuel Cell Electrocatalysts and Catalyst Layer: Fundamentals and Applications,* Second ed. London: Springer, pp. 99.

Spiegel, C. (2008), "PEM Fuel Cell Modeling and Simulation Using Matlab", Academic Press.

Stamenkovic, V.; Mun, B. S.; Mayrhofer, K. J. J.; Ross, P. N.; Markovic, N. M.; Rossmeisl, J.; Greeley, J. & Nørskov, J. K. (2006), "Changing the Activity of Electrocatalysts for Oxygen Reduction by Tuning the Surface Electronic Structure", Angewandte Chemie, 118, pp. 2963-2967.

Stamenkovic, V. R.; Mun, B. S.; Arenz, M.; Mayrhofer, K. J. J.; Lucas, C. a.; Wang, G.; Ross, P. N. & Markovic, N. M. (2007), "Trends in electrocatalysis on extended and nanoscale Pt-bimetallic alloy surfaces", Nature materials, 6, pp. 241-247.

Stolbov, S. & Ortigoza, M. A. (2012), "Rational Design of Competitive Electrocatalysts for Hydrogen Fuel Cells", The Journal of Physical Chemistry Letters, 3, pp. 463-467.

Subramanian, N. P.; Greszler, T. A.; Zhang, J.; Gu, W. & Makharia, R. (2012), "Pt-Oxide Coverage-Dependent Oxygen Reduction Reaction (ORR) Kinetics", Journal of the Electrochemical Society, 159, pp. B531-B531.

Vázquez-Huerta, G.; Ramos-Sánchez, G.; Rodríguez-Castellanos, A.; Meza-Calderón, D.; Antaño-López, R. & Solorza-Feria, O. (2010), "Electrochemical analysis of the kinetics and mechanism of the oxygen reduction reaction on Au nanoparticles", Journal of Electroanalytical Chemistry, 645, pp. 35-40.

Watanabe, M.; Tryk, D. a.; Wakisaka, M.; Yano, H. & Uchida, H. (2012), "Overview of recent developments in oxygen reduction electrocatalysis", Electrochimica Acta, 84, pp. 187-201.

Zhang, J.; Vukmirovic, M. B.; Xu, Y.; Mavrikakis, M. & Adzic, R. R. (2005), "Controlling the Catalytic Activity of Platinum-Monolayer Electrocatalysts for Oxygen Reduction with Different Substrates", Angewandte Chemie International Edition, 44, pp. 2132-2135.

Zhang, S.; Yuan, X.; Wang, H.; Merida, W.; Zhu, H.; Shen, J.; Wu, S. & Zhang, J. (2009), "A review of accelerated stress tests of MEA durability in PEM fuel cells", International Journal of Hydrogen Energy, 34, pp. 388-404.

Zhou, W. P.; Yang, X.; Vukmirovic, M. B.; Koel, B. E.; Jiao, J.; Peng, G.; Mavrikakis, M. & Adzic, R. R. (2009), "Improving electrocatalysts for O(2) reduction by fine-tuning the Pt-support interaction: Pt monolayer on the surfaces of a Pd(3)Fe(111) single-crystal alloy", Journal of the American Chemical Society, 131, pp. 12755-12762.

A. Alternative Model Derivations

Oxygen adsorption is rate limiting

$$i_{ORR} = \frac{nFAi_0 exp\left(-\alpha\frac{\eta}{f}\right)}{1 + {}^{1}/_{K_{2.11}K'\beta^4}}\left(\frac{1}{K_{2.11}K'\beta^4} - \frac{p_{O2}}{K_{2.10}}\right) \qquad (A.1)$$

Hydroxyl formation is rate limiting

$$i_{ORR} = nFAi_0 exp\left(-\alpha\frac{\eta}{f}\right)\left(\frac{1}{1 + {}^{K_{2.14}}/_{2}\,\beta + K_{2.10}\ K_{2.11}K_{2.14}\beta^3} - \frac{{}^{K'}/_{K2.14}\,p_{O2}\beta^3}{1 + {}^{K_{2.14}}/_{2}\,\beta + K_{2.10}\ K_{2.11}K_{2.14}\beta^3}\right) \qquad (A.2)$$

Hydroperoxyl formation with water desorption included is rate limiting

$$i_{ORR} = nFAi_0 exp\left(-\alpha\frac{\eta}{f}\right)\left(\frac{1}{{}^{1}/_{K'\beta^3}}\cdot\frac{1}{1 + {}^{1}/_{K'\beta^3} + K_{2.10}p_{O2}} - \frac{K"p_{O2}\beta}{1 + {}^{1}/_{K'\beta^3} + K_{2.10}p_{O2}}\right) \qquad (A.3)$$

B. Regressed Model Fits

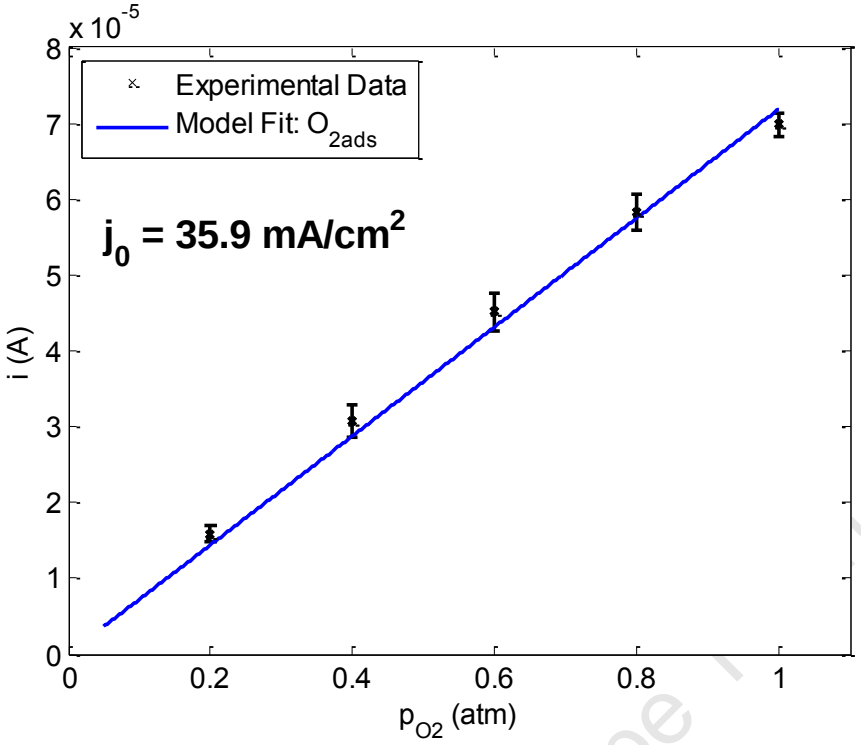

Figure A.1: Regressed fit for the $O_{2,ads}$ derived rate equation for experimentally derived kinetic current for constant absolute potential of 800 mV, 0.5 M H_2SO_4 and 25 °C.

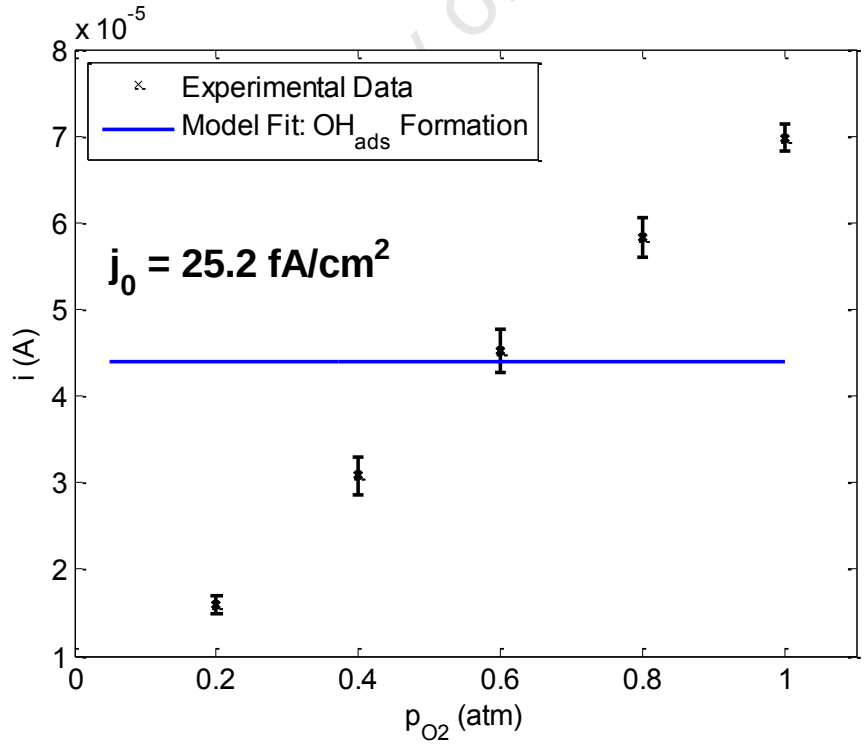

Figure A.2: Regressed fit for the OH_{ads} derived rate equation for experimentally derived kinetic current for constant absolute potential of 800 mV, 0.5 M H_2SO_4 and 25 °C.

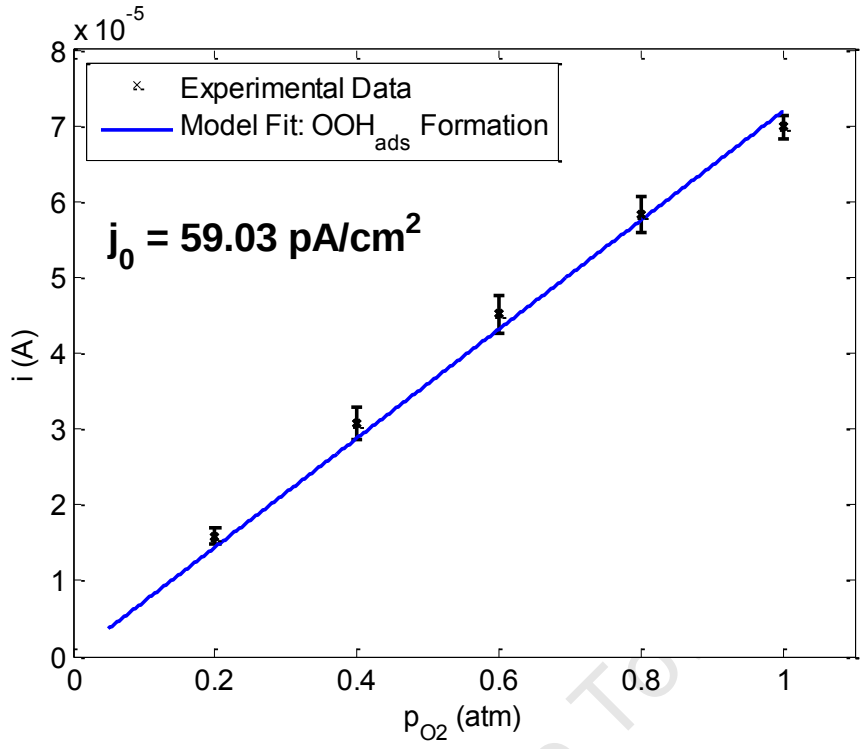

Figure A.3: Regressed fit for the OOH_{ads} derived rate equation for experimentally derived kinetic current for constant absolute potential of 800 mV, 0.5 M H_2SO_4 and 25 °C.

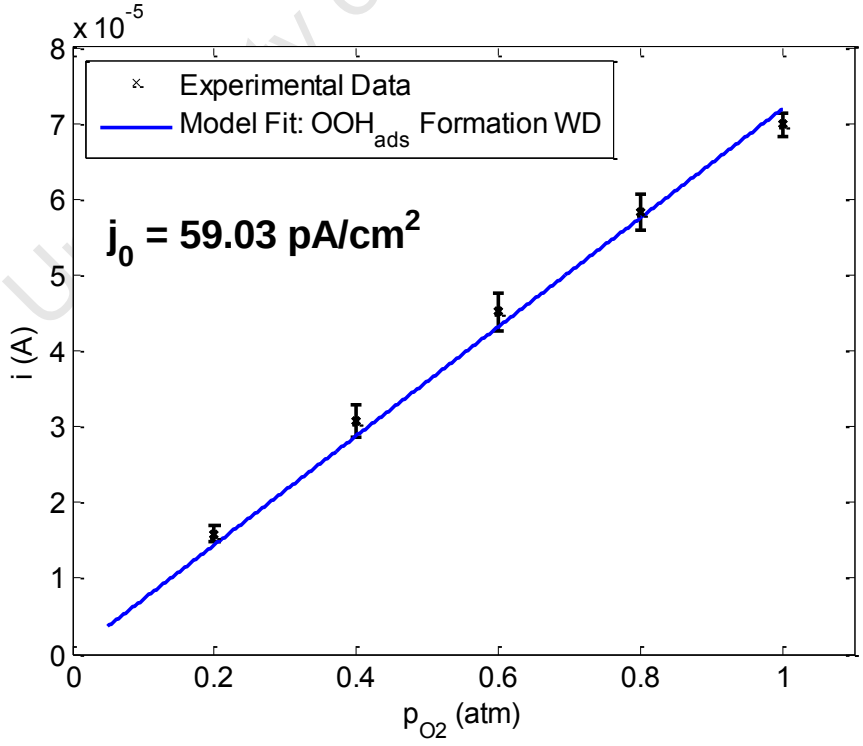

Figure A.4: Regressed fit for the OOH_{ads} (WD) derived rate equation for experimentally derived kinetic current for constant absolute potential of 800 mV, 0.5 M H_2SO_4 and 25 °C.

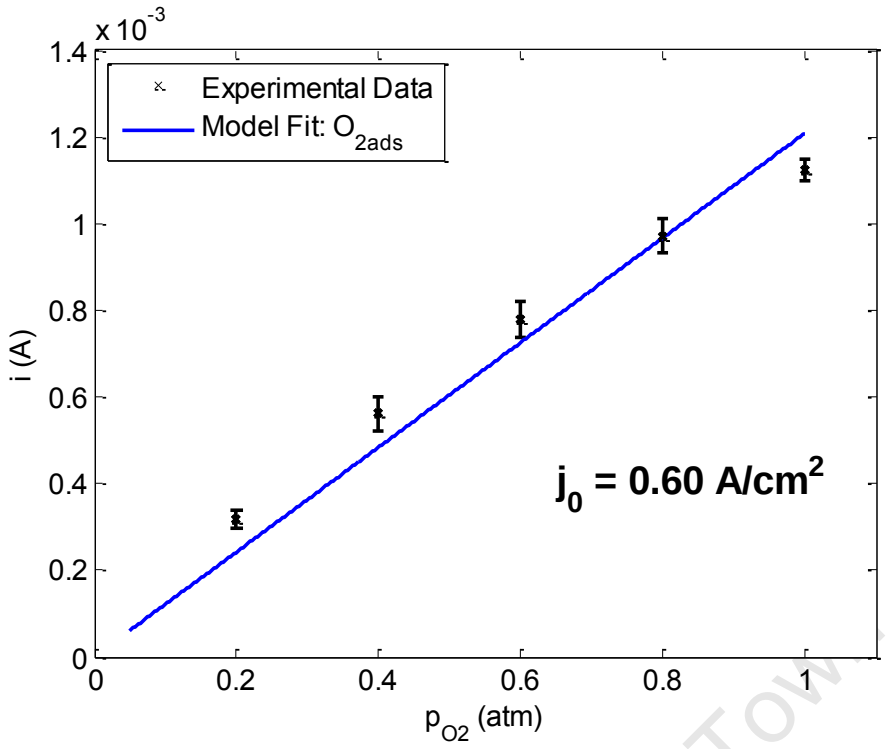

Figure A.5: Regressed fit for the $O_{2,ads}$ derived rate equation for experimentally derived kinetic current for constant overpotential of 430 mV, 0.5 M H_2SO_4 and 25 °C.

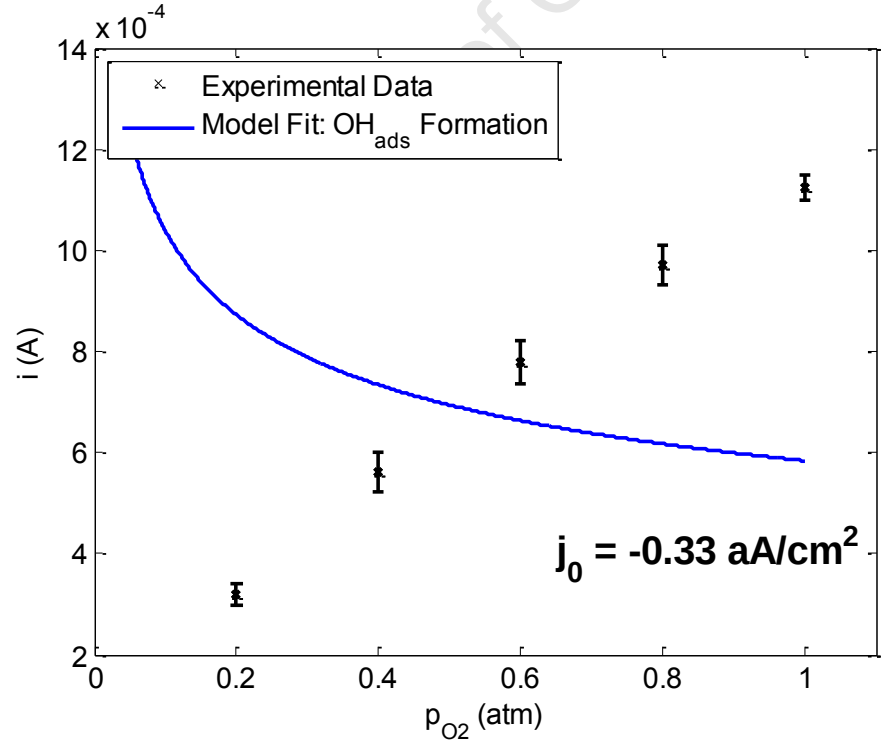

Figure A.6: Regressed fit for the OH_{ads} derived rate equation for experimentally derived kinetic current for constant overpotential of 430 mV, 0.5 M H_2SO_4 and 25 °C.

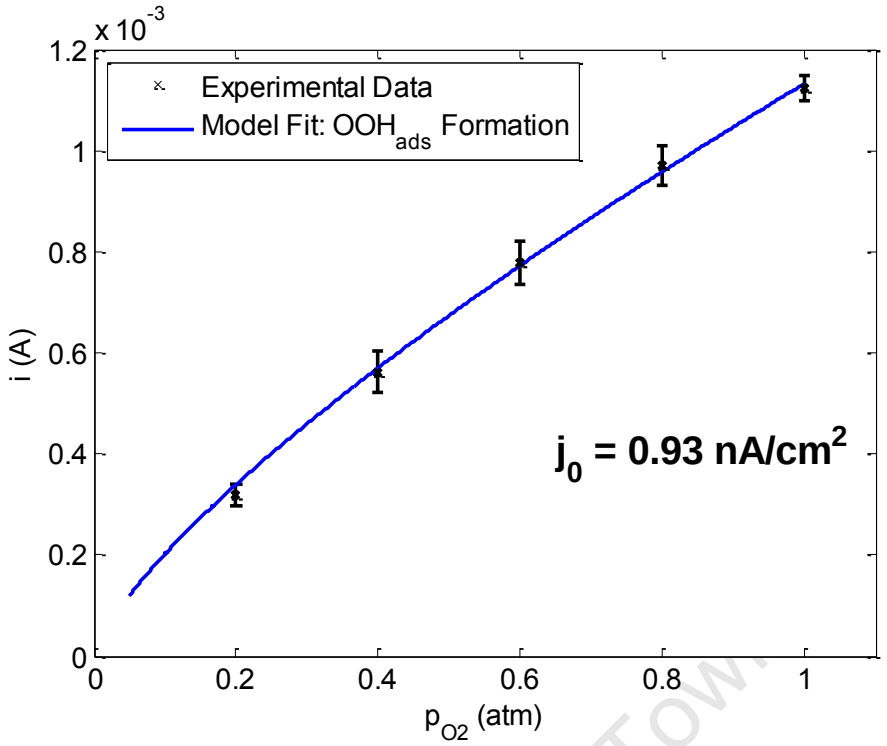

Figure A.7: Regressed fit for the OOH_{ads} derived rate equation for experimentally derived kinetic current for constant overpotential of 430 mV, 0.5 M H_2SO_4 and 25 °C.

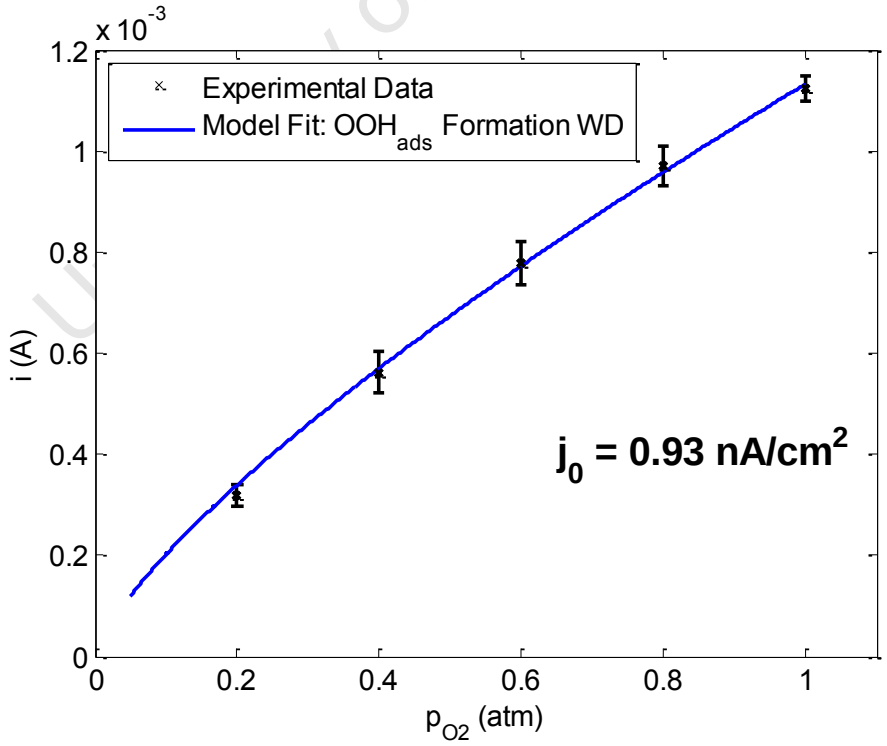

Figure A.8: Regressed fit for the OOH_{ads} (WD) derived rate equation for experimentally derived kinetic current for constant overpotential of 430 mV, 0.5 M H_2SO_4 and 25 °C.

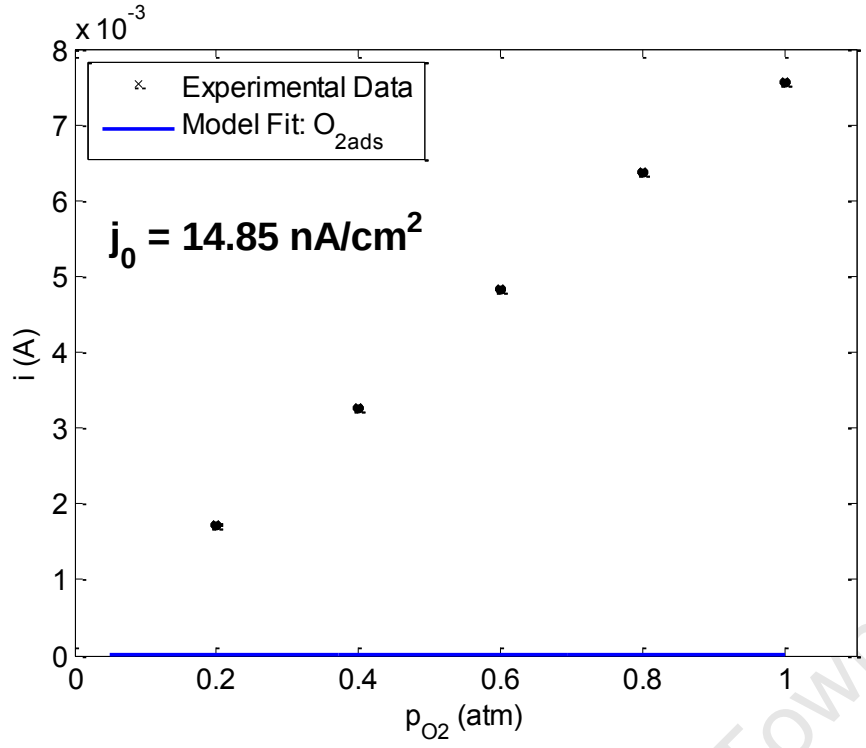

Figure A.9: Regressed fit for the $O_{2,ads}$ derived rate equation for experimentally derived kinetic current for constant absolute potential of 700 mV, 0.5 M H_2SO_4 and 25 °C.

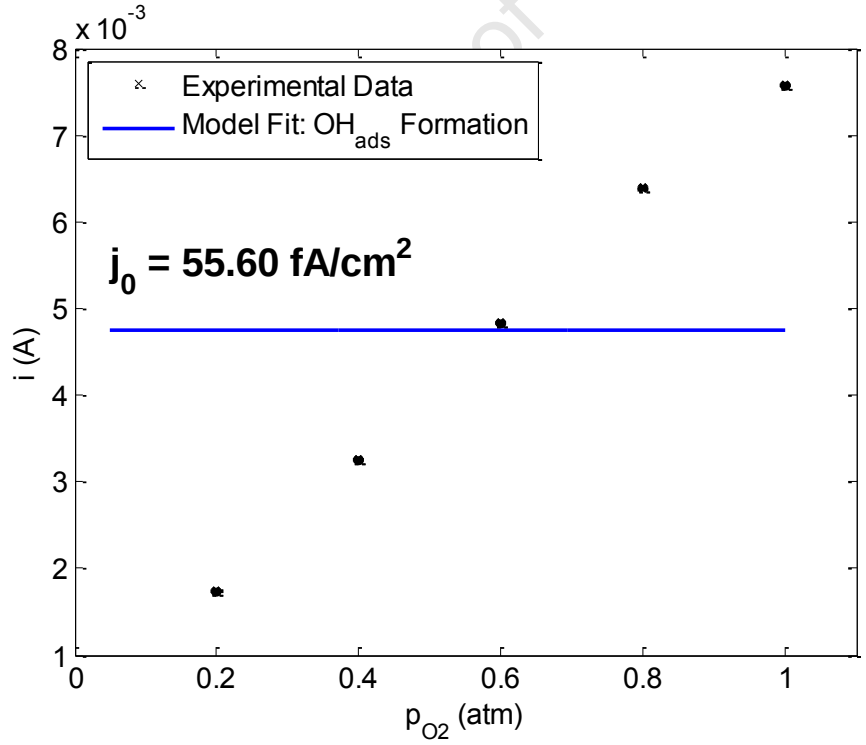

Figure A.10: Regressed fit for the OH_{ads} derived rate equation for experimentally derived kinetic current for constant absolute potential of 700 mV, 0.5 M H_2SO_4 and 25 °C.

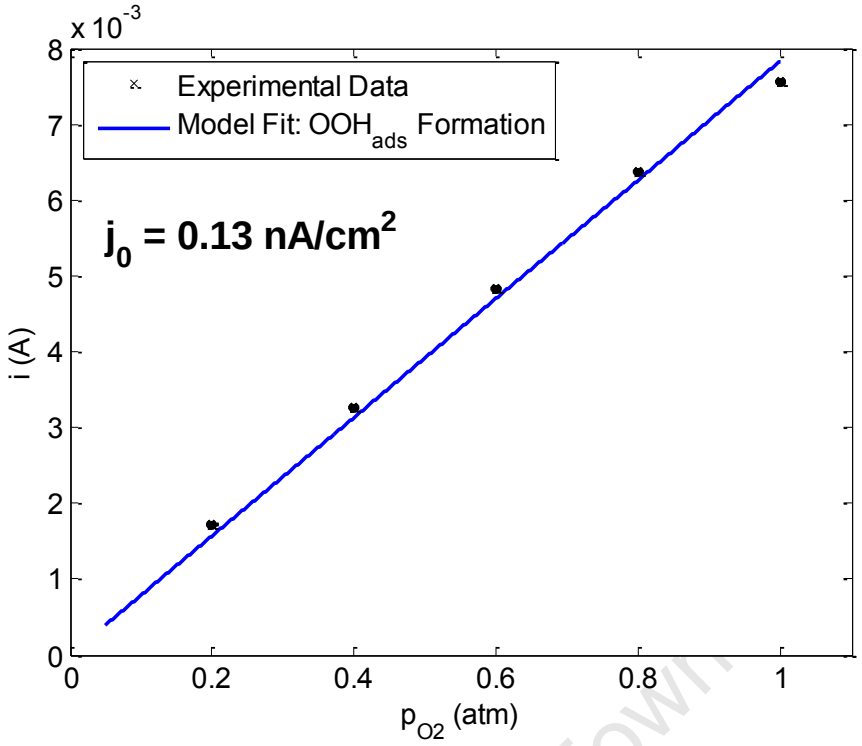

Figure A.11: Regressed fit for the OOH_{ads} derived rate equation for experimentally derived kinetic current for constant absolute potential of 700 mV, 0.5 M H_2SO_4 and 25 °C.

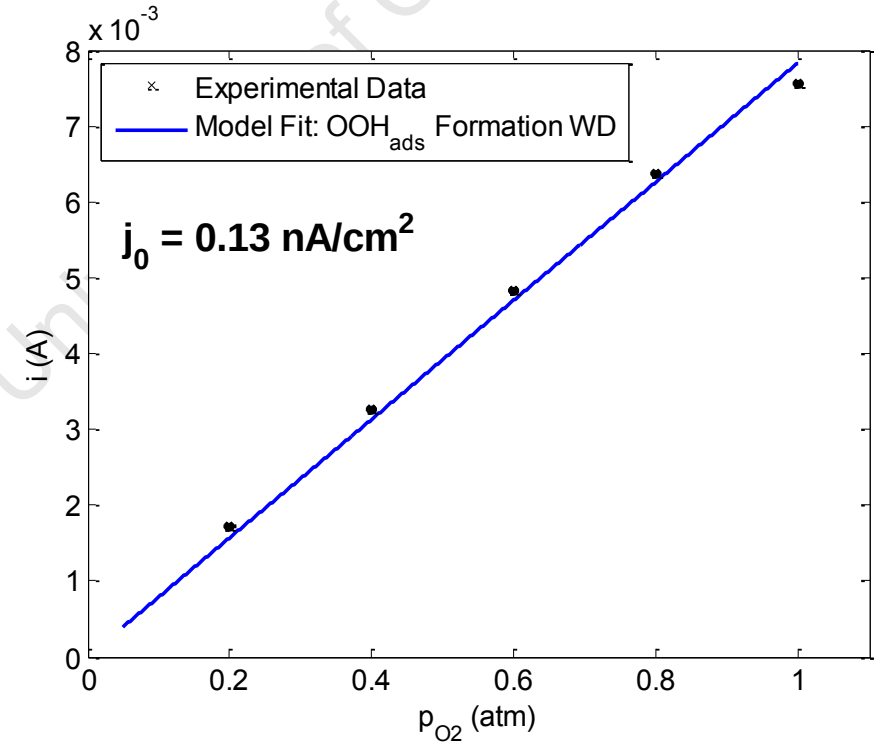

Figure A.12: Regressed fit for the OOH_{ads} (WD) derived rate equation for experimentally derived kinetic current for constant absolute potential of 700 mV, 0.5 M H_2SO_4 and 25 °C.

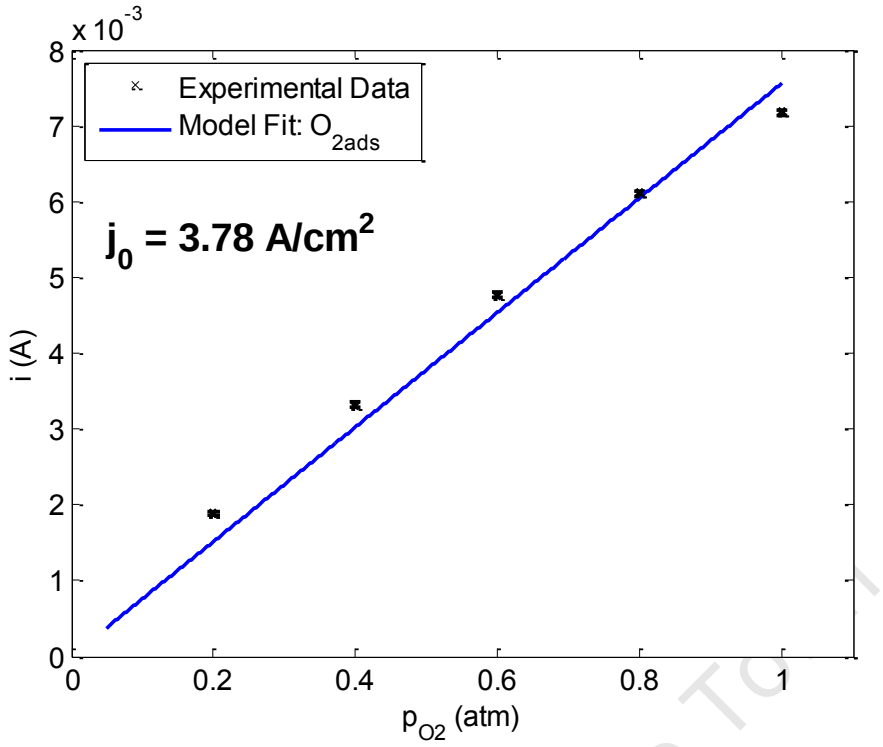

Figure A.13: Regressed fit for the $O_{2,ads}$ derived rate equation for experimentally derived kinetic current for constant overpotential of 530 mV, 0.5 M H_2SO_4 and 25 °C.

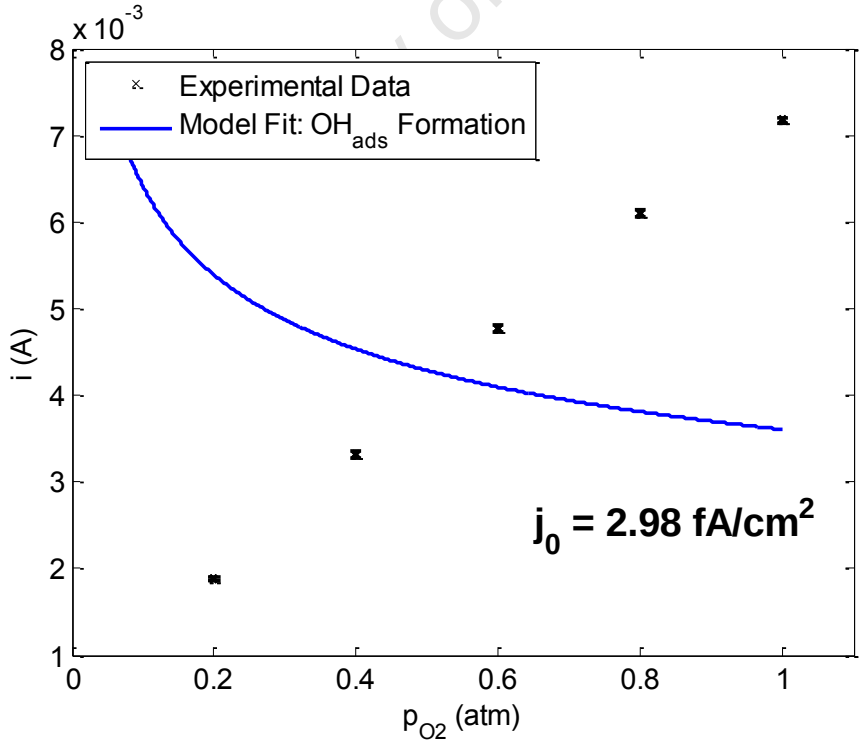

Figure A.14: Regressed fit for the OH_{ads} derived rate equation for experimentally derived kinetic current for constant overpotential of 530 mV, 0.5 M H_2SO_4 and 25 °C.

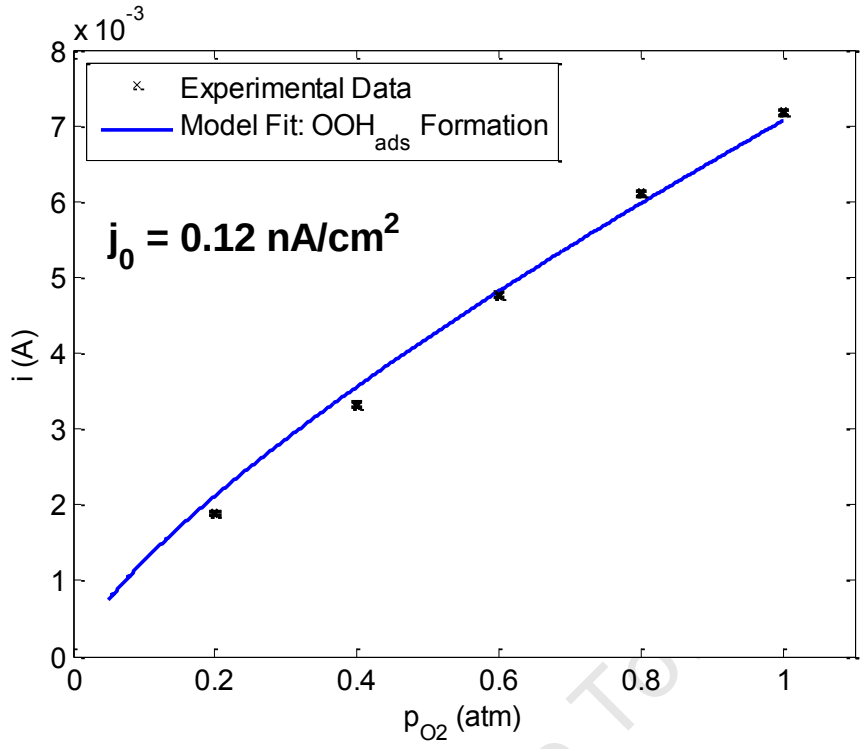

Figure A.15: Regressed fit for the OOH_{ads} derived rate equation for experimentally derived kinetic current for constant overpotential of 530 mV, 0.5 M H_2SO_4 and 25 °C.

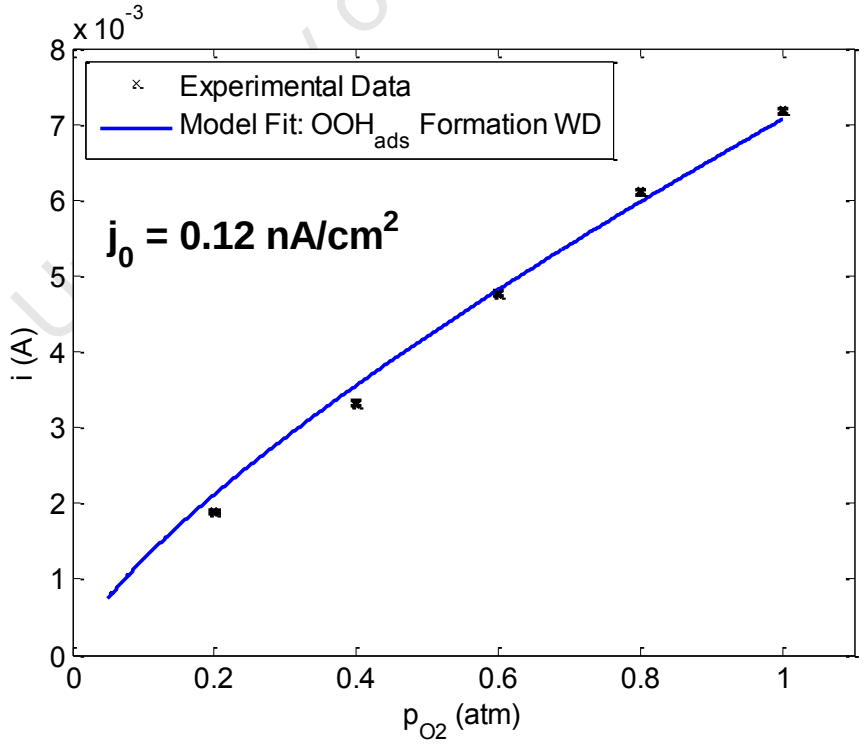

Figure A.16: Regressed fit for the OOH_{ads} (WD) derived rate equation for experimentally derived kinetic current for constant overpotential of 530 mV, 0.5 M H_2SO_4 and 25 °C.

C. Experimental Curves

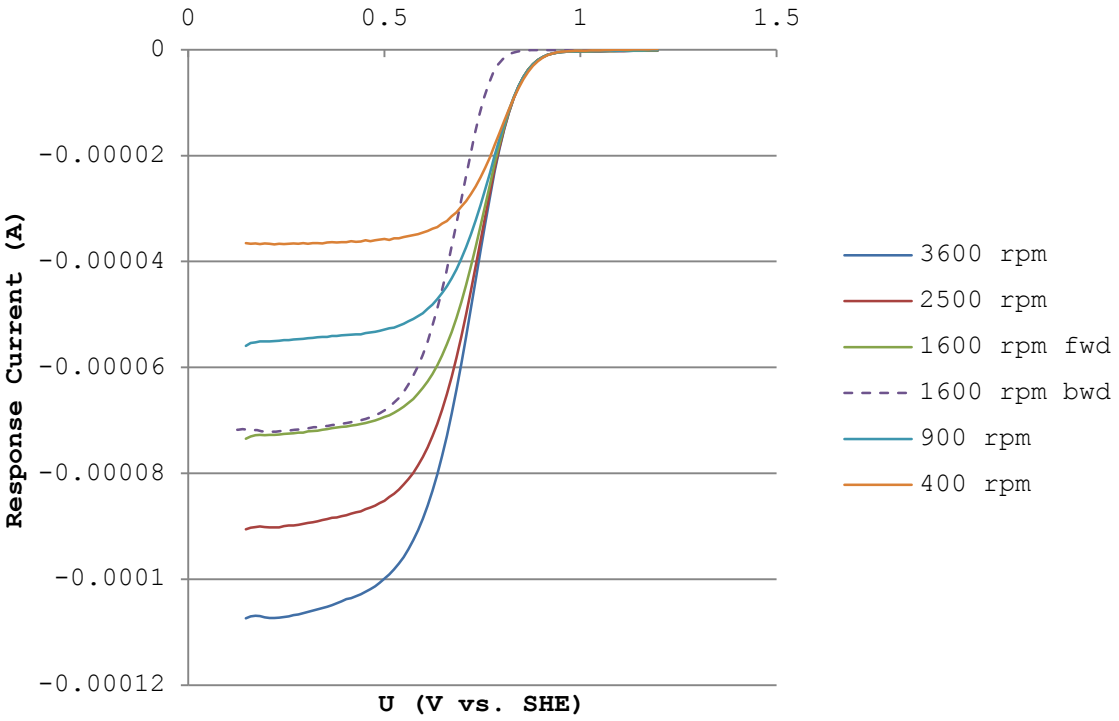

Figure A.17: Background-corrected polarisation curves of ORR on polycrystalline Pt at a sweep rate of 20 mV/s at 25 °C in 0.5 M H_2SO_4 under 20% O_2-saturated. Solid lines represent upward going sweeps and only downward going sweeps at 1600 rpm are shown by the dotted line.

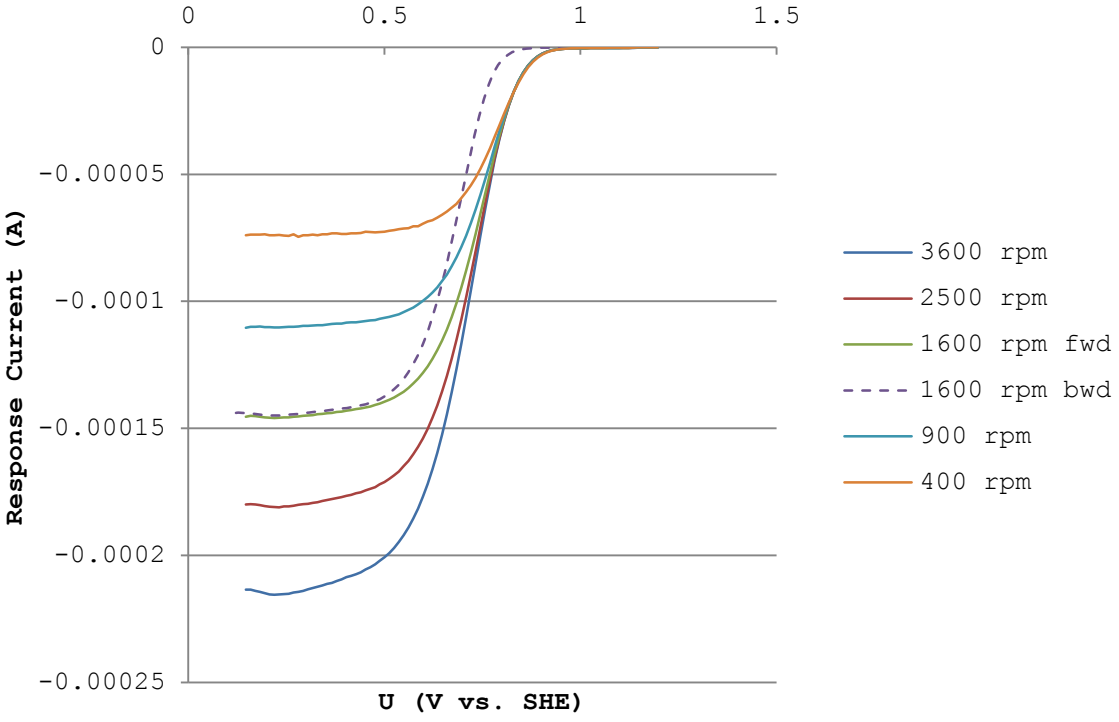

Figure A.18: Background-corrected polarisation curves of ORR on polycrystalline Pt at a sweep rate of 20 mV/s at 25 °C in 0.5 M H_2SO_4 under 40% O_2-saturated. Solid lines represent upward going sweeps and only downward going sweeps at 1600 rpm are shown by the dotted line.

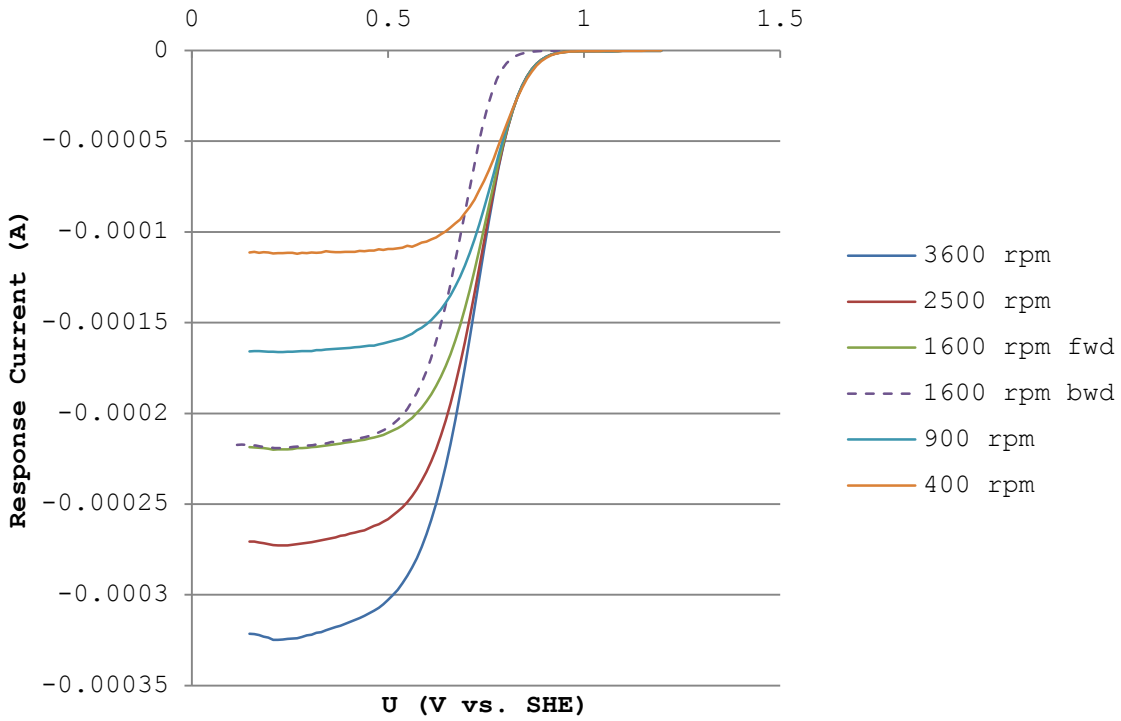

Figure A.19: Background-corrected polarisation curves of ORR on polycrystalline Pt at a sweep rate of 20 mV/s at 25 °C in 0.5 M H_2SO_4 under 60% O_2-saturated. Solid lines represent upward going sweeps and only downward going sweeps at 1600 rpm are shown by the dotted line.

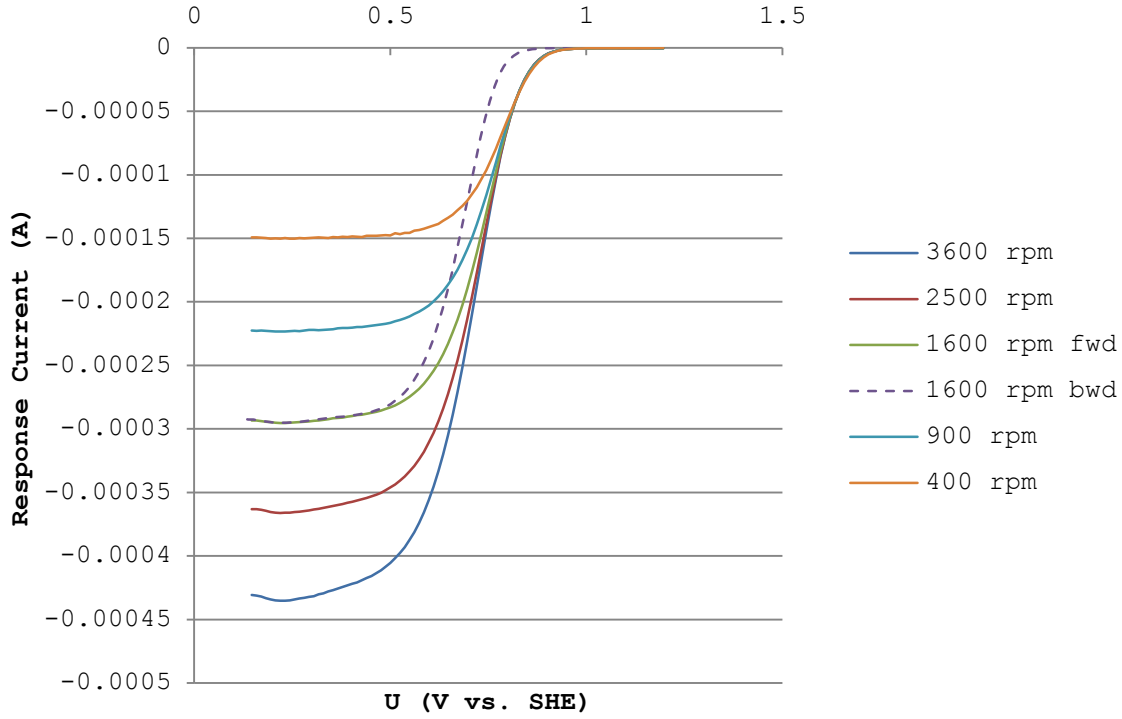

Figure A.20: Background-corrected polarisation curves of ORR on polycrystalline Pt at a sweep rate of 20 mV/s at 25 °C in 0.5 M H_2SO_4 under 80% O_2-saturated. Solid lines represent upward going sweeps and only downward going sweeps at 1600 rpm are shown by the dotted line.

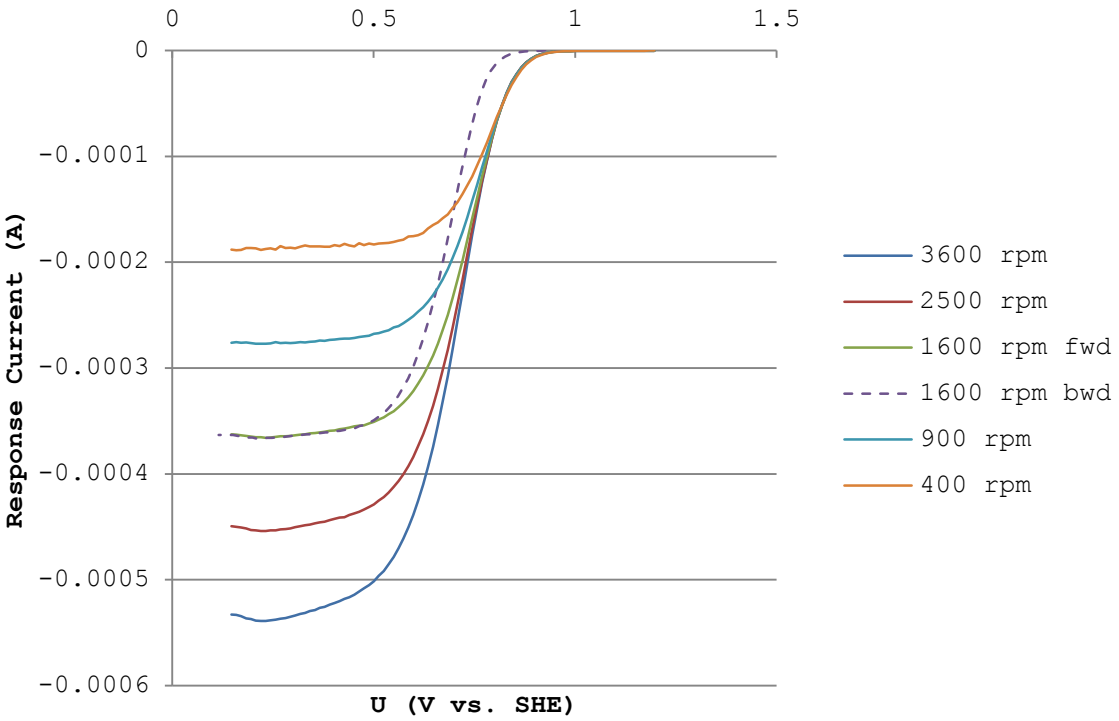

Figure A.21: Background-corrected polarisation curves of ORR on polycrystalline Pt at a sweep rate of 20 mV/s at 25 °C in 0.5 M H_2SO_4 under 100% O_2-saturated. Solid lines represent upward going sweeps and only downward going sweeps at 1600 rpm are shown by the dotted line.

List of Symbols

$O_2 + * \rightleftharpoons O_2*$ (2.10)

$O_2* + (H^+ + e^-) \rightleftharpoons HO_2*$ **(2.11)**

$HO_2* + (H^+ + e^-) \rightleftharpoons H_2O + O*$ (2.12)

$O* + (H^+ + e^-) \rightleftharpoons HO*$ (2.13)

$HO* + (H^+ + e^-) \rightleftharpoons H_2O + *$ (2.14)

$H_2O* \rightleftharpoons H_2O + *$ *(2.15)*

A	geometric area
K	equilibrium constant
T	temperature
a	species activity
c	concentration
f	F/RT
i	current
i_0	exchange current
k	rate constant
n	number of electrons
p	pressure, partial
r	rate of reaction
α	transfer coefficient
η	potential, over
θ	reaction site
*	reaction site